

Analysis of fermions on a honeycomb bilayer lattice with finite-range interactions in the weak-coupling limit

Robert E. Throckmorton¹ and Oskar Vafek¹

¹*National High Magnetic Field Laboratory and Department of Physics,
Florida State University, Tallahassee, Florida 32306, USA*

(Dated: October 23, 2019)

We extend previous analyses of fermions on a honeycomb bilayer lattice via weak-coupling renormalization group (RG) methods with extremely short-range and extremely long-range interactions to the case of finite-range interactions. In particular, we consider different types of interactions including screened Coulomb interactions, much like those produced by a point charge placed either above a single infinite conducting plate or exactly halfway between two parallel infinite conducting plates. Our considerations are motivated by the fact that, in some recent experiments on bilayer graphene^{1,2} there is a single gate while in others^{3,4}, there are two gates, which can function as the conducting planes and which, we argue, can lead to distinct broken symmetry phases. We map out the phases that the system enters as a function of the range of the interaction. For spin- $\frac{1}{2}$ fermions, we discover that the system enters an antiferromagnetic phase for short ranges of the interaction and a nematic phase at long ranges, in agreement with Refs.⁵ and⁶. While the antiferromagnetic phase results in a gap in the spectrum, the nematic phase is gapless, splitting the quadratic degeneracy points into two Dirac cones each^{5,7}. Our results can help reconcile the recent results of two seemingly contradictory experiments^{2,4}. We also consider the effects of an applied magnetic field on the system in the antiferromagnetic phase via variational mean field theory, obtaining results in qualitative agreement with the experimental data. We find that the antiferromagnetic order parameter increases with field, at first quadratically at low fields, then as $B/\ln(B/B_0)$ at higher fields. For spinless fermions, we find that the system enters a layer-polarized state for short ranges of the interaction, in agreement with Ref.⁶. As we increase the interaction range, the system enters a quantum anomalous Hall state, followed by a Kekulé state, and may return back to the layer-polarized state for long ranges.

I. INTRODUCTION

The problem of interacting fermions on an A-B stacked honeycomb bilayer lattice has been of great interest, both theoretically and experimentally, due in no small part to its band structure. Typically, the band structure possesses two inequivalent points, labeled \mathbf{K} and $\mathbf{K}' = -\mathbf{K}$, in the Brillouin zone at which the two low-energy bands make contact at four Dirac-like cones⁸. However, in the case where we neglect all but nearest-neighbor hopping terms, these four Dirac cones merge into a single quadratic degeneracy point⁸. The density of states at the Fermi level at half-filling therefore becomes finite in this special case. This leads to logarithmic divergences in the uniform and static susceptibilities to various symmetry-breaking orders at zero temperature^{5,6}, and thus we expect such phases to appear for arbitrarily weak interactions over some finite range of temperatures.

One key motivation for the study of the honeycomb bilayer in particular is the fact that bilayer graphene, a material of great interest, possesses this lattice structure. In particular, measurements of the conductivity of suspended bilayer graphene in various external electric and magnetic fields as well as different carrier densities³, followed by compressibility measurements¹, provide evidence suggesting that a symmetry-breaking state appears; the two possible states argued for in these works are an anomalous quantum Hall phase, in which the system develops a non-zero quantized Hall conductivity in

the absence of a magnetic field, and a nematic phase, in which the quadratic degeneracy points each split into two massless Dirac-like cones. A more recent experiment² finds evidence for the presence of a nematic phase^{5,7} by measuring the width of a peak in the resistivity as a function of the carrier density at different temperatures and by measuring cyclotron gaps as a function of the applied magnetic field for different filling factors. Another, even more recent, experiment⁴ uses measurements of two-terminal conductance to argue for a state in which the system develops an energy gap in its spectrum, in apparent disagreement with the previous experiment, since the nematic state is gapless. Two of these experiments^{3,4} were performed with a top and a bottom gate, while the other two^{1,2} are performed with only a single (bottom) gate; in the former, the external electric field could be controlled independently of the carrier density. The results of the doubly gated experiments imply that the symmetry breaking order can be suppressed by the application of a non-zero external electric field, E_{\perp} , thus ruling out the possibility of a layer-polarized state as the particular order that is observed. It should also be noted that strain has qualitatively identical effects on the electronic spectrum as the presence of a nematic order⁹; this, however, was ruled out as the cause of the effects observed in Ref.² on the grounds that the observed effects were too large to be accounted for by strain and that the same features are observed in four different samples where the externally induced strain is expected to vary.

In addition to experimental investigations, there have also been a number of theoretical investigations regarding the nature of the symmetry-breaking states of the A-B stacked honeycomb bilayer. One such investigation¹⁰ uses variational methods to argue for a ferromagnetic phase for long-range interactions and arguments based on susceptibility calculations and a mean-field calculation to argue for an antiferromagnetic phase for short-range interactions. Two other works employ a mean-field approach to argue for a “(layer) pseudospin magnet” state¹¹ and a ferromagnetic state¹², while later investigations argue for a layer-polarized state¹³ within the mean-field approximation and a quantum anomalous Hall state¹⁴ with mean field plus Gaussian fluctuations. Another work by the same group¹⁵ considers the phase of the system within the mean-field approximation as a function of external electric and magnetic fields and finds a quantum anomalous Hall state, a quantum Hall ferromagnetic insulator, and a layer-polarized state. A very recent investigation arrives at a “(layer) pseudospin antiferromagnetic” state for the honeycomb bilayer¹⁶.

The mean-field approach, however, has one major disadvantage. It does not treat the leading logarithmic divergences that appear in perturbation theory correctly. On the other hand, the renormalization group (RG) approach does; it essentially re-sums a class of diagrams corresponding to the leading logarithmic divergences at each order. An example of this point is provided by the treatment of interacting fermions on a one-dimensional chain¹⁷; in this case, mean field theory predicts that there will be a charge density wave state for arbitrarily weak interactions, while RG predicts a Luttinger liquid for weak interactions. We therefore believe that RG is more accurate as a means of predicting the state that our system enters than a mean field approach. There are now several papers that employ the RG approach in studying the honeycomb bilayer in the weak-coupling limit^{5-7,18}.

A paper by one of us and Yang⁵ uses this method to argue for the existence of a nematic state for extremely long-range interactions in the case of spin- $\frac{1}{2}$ fermions, and a similar paper by Lemonik *et. al.*⁷ which followed comes to the same conclusion. Another paper by one of us⁶ investigates the extremely short-range limit using the same approach, and finds that a system of spinless fermions will enter a layer-polarized state, while spin- $\frac{1}{2}$ fermions will enter an antiferromagnetic state; it is also argued within that these same states should persist even in the strong-coupling limit.

In the present work, we will extend the analyses conducted in Refs.⁶ and⁵ to the case of finite-ranged density-density interactions, and we will consider both spinless and spin- $\frac{1}{2}$ fermions. In particular, we consider several types of interactions including 1) screened Coulomb interactions, much like those produced by a point charge placed exactly halfway between two parallel infinite conducting plates, 2) same as 1) but for a single infinite conducting plate and 3) for an exponentially decaying interaction. The forms considered include a parameter

ξ that is proportional to the range of the interaction. For all cases, we generate phase diagrams showing what phase the system enters as a function of ξ .

Our procedure for the calculation is as follows. We start with a tight-binding lattice model for the honeycomb bilayer with a density-density interaction between electrons. From this, we may derive a low-energy effective field theory, which takes the same form as that given in the previous work⁶; said field theory contains 9 different contact quartic couplings that are allowed by the symmetries of the honeycomb bilayer lattice and by Fierz identities. We find the values of the coupling constants in terms of the interaction in our original tight-binding lattice microscopic model. We then use these values as the initial conditions for the RG flow equations derived in Ref.⁶, which we integrate numerically. We find that, at a certain scale, the coupling constants diverge; we associate this divergence with the appearance of a symmetry-breaking order. While the coupling constants themselves diverge, the ratios of these constants approach finite values. We may therefore think of different ordering tendencies as corresponding to fixed points in an 8-dimensional ratio space. In what follows, the term, “fixed point”, will refer to fixed points in ratio space.

To determine the nature of the order, we first introduce symmetry-breaking source terms into our theory, and then determine how they flow under RG. We then determine which one diverges most rapidly as we approach the point at which our coupling constants diverge; we take the order associated with the most rapidly diverging source term to be the one present in the system. In the case of spinless fermions, we stop the flows of our coupling constants just before the point at which they diverge; in this case all of the fixed points that we approach are completely stable. On the other hand, we find that not all of the fixed points that we approach in the spin- $\frac{1}{2}$ case are stable. In particular, the nematic fixed point found in the previous work⁵, while stable within the two-dimensional subspace considered therein, turns out to have two unstable directions in the full 8-dimensional ratio space. However, our numerical results suggest that this fixed point has a large basin of influence in the sense that our flows are attracted toward this fixed point until just before they reach it, at which point the couplings become large and their ratios begin to move away from the fixed point. Because of this and the fact that our RG equations are only valid for weak coupling, in the spin- $\frac{1}{2}$ case, we stop the flows of our dimensionless coupling constants when one of them reaches a fixed cutoff ≈ 0.1 . Because we do this, rather than stop the flows just before the coupling constants diverge, we have another axis in our phase diagram for the case of spin $\frac{1}{2}$ Fermions, namely the strength of the initial couplings.

Our results for the spinless case are summarized in Figure 1. We find that, for $\xi < \xi_1$, the system enters a layer-polarized state, in agreement with the previous work⁶. As we increase ξ , the system enters an anomalous quantum Hall state above the stated range, followed

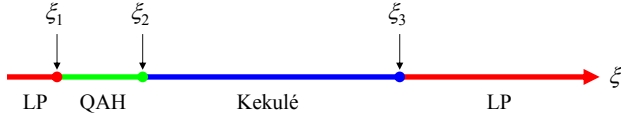


FIG. 1: Phase diagram for spinless fermions on a honeycomb bilayer lattice, as a function of the interaction range ξ . For $\xi < \xi_1$, the system is in a layer-polarized (LP) state. As we increase ξ , the system will enter a quantum anomalous Hall (QAH) state for $\xi_1 < \xi < \xi_2$, followed by a Kekulé state for $\xi_2 < \xi < \xi_3$. Finally, for $\xi > \xi_3$, the system re-enters the layer-polarized state. The values of ξ_1 , ξ_2 , and ξ_3 depend on the form of the interaction considered.

by a Kekulé state for $\xi > \xi_2$. The Kekulé state breaks translational symmetry by modifying the tight-binding hopping terms in a regular pattern. Unlike the case of a single-layer honeycomb lattice¹⁹, however, the modifications to the tight-binding hopping terms are purely imaginary, and therefore the Kekulé state in a honeycomb bilayer also breaks time reversal symmetry. If we increase the range even further, the system will go back into the layer-polarized state for $\xi > \xi_3$. The values of ξ_1 , ξ_2 , and ξ_3 depend on the form of the interaction considered. For the screened Coulomb-like interaction, $\xi_1 = 0.396a$, where a is the lattice constant, $\xi_2 = 21.05a$, and $\xi_3 = 119.73a$. For the exponential interaction, $\xi_1 = 0.392a$ and $\xi_2 = 12.01a$. In this case, we did not see a transition back into the layer-polarized state for any $\xi \leq 800a$, so that, if such a transition does occur, it will happen at some value of $\xi_3 > 800a$.

Our results for the spin- $\frac{1}{2}$ case for monotonically decreasing repulsive interactions are summarized in Figure 2. For small values of ξ , we find that the system enters the antiferromagnetic phase, while, for long ranges, the system enters the nematic phase, again in agreement with the previous work^{5,6}. The value of ξ at which we enter the nematic phase may vary from $\xi \approx 100a$ to $\xi \approx 1500a$.

For the dipole-like potential, much like the one that is produced by a point charge a distance ξ above a single infinite conducting plate,

$$V(\mathbf{r}) = U_0 \left[\frac{1}{r/\xi} - \frac{1}{\sqrt{(r/\xi)^2 + 1}} \right], \quad (1)$$

where U_0 is a sufficiently small constant, so that our system is at weak coupling. For the potential produced by a point charge placed exactly half-way and distance ξ between two infinite conducting plates

$$V(\mathbf{r}) = 4U_0 \sum_{k=0}^{\infty} K_0 \left[(2k+1)\pi \frac{r}{\xi} \right] \approx U_0 \frac{2\sqrt{2}e^{-\pi r/\xi}}{\sqrt{r/\xi}}, \quad (2)$$

where $K_n(x)$ is the modified Bessel function and the last equation holds asymptotically at large values of r/ξ . Note that these expressions, as they are, diverge at $\mathbf{r} = 0$ —that is, they diverge for two electrons on

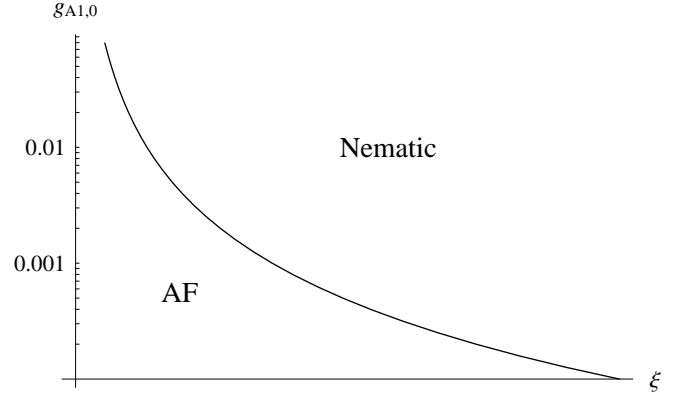


FIG. 2: Schematic phase diagram for spin- $\frac{1}{2}$ fermions on a honeycomb bilayer lattice, as a function of the interaction range ξ and the initial strength of one of the dimensionless coupling constants $g_{A_1}^0$ for several functional forms of interaction discussed in the text. In each case, the electron-electron repulsion is monotonically decreasing and the on-site electron-electron repulsion is greater than the nearest-neighbor repulsion. For short-ranged interactions, we find an antiferromagnetic (AF) phase, while, for long-range interactions, we find a nematic phase. Interestingly, if we make the on-site interaction *weaker* than the nearest-neighbor interaction, we may also find a quantum spin Hall phase for intermediate ranges.

the same lattice site. Because of this, and due to the fact that the electrons in the tight-binding model cannot, strictly speaking, be considered point particles, we render these on-site interactions finite by setting said interactions equal to a constant λ times the nearest-neighbor interaction; our main results were found for $\lambda = 1.2$; this choice makes our interactions monotonically decreasing with distance. We also considered a few cases where $\lambda < 1$, which we discuss further in the text.

The phase diagram comparing these two cases is shown in Fig.4. In each case, we find a qualitatively identical phase diagram, except that the value of ξ at which the transition from the antiferromagnetic state to the nematic state occurs for a given initial value of the coupling constant g_{A_1} in the single conducting plane case is roughly half of what it would be in the case of two conducting planes. These results could help explain why the experiments mentioned earlier^{2,4} find evidence for different broken symmetry phases. In the first experiment², there is only a single gate present and as a result the electron-electron interaction is longer ranged than in the second experiment⁴, where there are two gates. When the electrons experience a longer range interaction, the nematic phase is favored, while, when the interactions are short-ranged the antiferromagnetic phase is favored.

Another way to think of our results is as follows. When we make our interactions longer-ranged in real space, we are, at the same time, making them shorter-ranged in momentum space. Let us start with a density-density interaction of the general form, $\sum_{\mathbf{r}, \mathbf{r}'} V(\mathbf{r} - \mathbf{r}') n(\mathbf{r}) n(\mathbf{r}')$, where $n(\mathbf{r}) = \sum_{\sigma} c_{\sigma}^{\dagger}(\mathbf{r}) c_{\sigma}(\mathbf{r})$. It turns out that the initial

couplings in the effective low-energy field theory depend on the Fourier components $V(\mathbf{q})$ of this interaction at $\mathbf{q} = 0$ and $\mathbf{q} = 2\mathbf{K}$; we will label these components as V_0 and V_{2K} , respectively. In the case of a long-range interaction $V_0 \gg V_{2K}$, and said interaction will therefore mostly cause forward scattering of the electrons while, in the case of a short-range interaction, V_{2K} will become comparable to V_0 , and thus back scattering begins to become comparable to the forward scattering. We would therefore say that, in the spin- $\frac{1}{2}$ case, we obtain a nematic phase when forward scattering dominates, while we obtain an antiferromagnetic phase when back scattering becomes comparable to the forward scattering.

Interestingly, if we make the on-site interaction *weaker* than the nearest-neighbor interaction, we may also obtain a quantum spin Hall phase for intermediate ranges of the interaction; whether or not it appears depends on the sign of one of our coupling constants, g_β , which we define in the main text, for a given value of ξ .

We were, however, unable to obtain a quantum anomalous Hall state in this case with any density-density interaction. Therefore, we consider what form of an additional interaction could be added in order to produce this state; our motivation for doing so will be stated in the main text.

Motivated by experimental data⁴ and by our above conclusions, we then turn our attention to investigating the effects of an applied magnetic field on the antiferromagnetic phase. A similar calculation has already been performed²⁰, in which a self-consistent mean field approach is employed, and a second order parameter is introduced. Our analysis includes only the antiferromagnetic order parameter, and employs variational mean field methods. The equation that we obtain for this order parameter has the same form as in Ref.²⁰, but there are important qualitative differences between the results given therein and our results.

In our method of solution, we eliminate the coupling constants in the problem by rewriting the self-consistent equation in terms of the measurable order parameter at zero field Δ_0 which allows us to send the energy cutoff in our problem to infinity. By doing so, we can obtain the scaling equation for the order parameter at finite B-field *whose dependence on coupling constants enters entirely through Δ_0* :

$$I(\alpha) + \frac{1}{|\alpha|} - \ln\left(1 + \sqrt{\alpha^2 + \frac{3}{4}}\right) = \ln \beta, \quad (3)$$

where $\alpha = \Delta(B)/\omega_c$, $\beta = \omega_c/\Delta_0$, $\Delta(B)$ is the order parameter at finite field, ω_c is the cyclotron frequency of the electrons in our system, $I(\alpha)$ may be very accurately approximated as

$$I(\alpha) \approx -\frac{2}{\left[\left(-\frac{1}{2}I(0)\right)^{-2/3} + 4 \cdot 6^{2/3}\alpha^2\right]^{3/2}}, \quad (4)$$

and $I(0) \approx -0.0503$ is the exact value of $I(\alpha)$ at $\alpha = 0$.

Note that this scaling form demands that, if the dependence of $\Delta(B)$ on B were linear, as is reported in Ref.⁴,

then the slope is *independent of the coupling constants in the theory* since Δ_0 has to cancel on both sides of the equation. This differs from Ref.²⁰ where even for the AF order alone, the slope is non-universal and depends on the dimensionless coupling constant as can be seen from their Equation (10). Still, we find that there is no regime in which the solution of the above scaling equations is strictly linear. For low fields, the order parameter has a quadratic dependence on the magnetic field,

$$\Delta(B) = \Delta_0 + \frac{\omega_c^2}{8\Delta_0}, \quad (5)$$

while, at high magnetic fields, the dependence on the field is

$$\Delta(B) = \frac{\omega_c}{\ln(\omega_c/\Delta_0) + C}, \quad (6)$$

where $C \approx 0.67$. This may be experimentally hard to distinguish from linear dependence. The gap, which is simply $2\Delta(B)$ in our case, therefore has the same dependence on the magnetic field.

While our results agree qualitatively with the experiment of Ref.⁴, they do not agree quantitatively. We find that the coefficient of B^2 in our low-field approximation is smaller than what is observed by a factor of ~ 4 , while the maximum slope of our curve is smaller by a factor of ~ 2 than the experimentally-observed slope at high fields. In addition, the experimental data shows quantum Hall plateaus, namely $\nu = 1$ and $\nu = 3$, that cannot be explained by the presence of an antiferromagnetic order parameter alone, even if we account for Zeeman splitting⁴. This suggests that some other order emerges in the presence of an applied magnetic field, and that this order will change the predicted energy gap to more closely follow the experimental data.

The rest of the paper is organized as follows. In Sections II and III, we consider spinless and spin- $\frac{1}{2}$ fermions on a honeycomb bilayer lattice, respectively. In each case, we write down the microscopic lattice model Hamiltonian, obtain the effective low-energy theory, and then present the RG analysis of each theory. In Section IV, we present our variational mean field analysis of the antiferromagnetic state in the presence of an applied magnetic field. We present our conclusions in Section V, and provide mathematical details in the appendix.

II. SPINLESS CASE

A. Starting Hamiltonian

Our starting point will be a tight-binding A-B stacked honeycomb bilayer lattice with only nearest-neighbor hopping terms and a two-particle interaction; the lattice and the corresponding reciprocal momentum (\mathbf{k}) space is illustrated in Figure 3. By including only nearest-neighbor hopping, we are fine-tuning our system so that

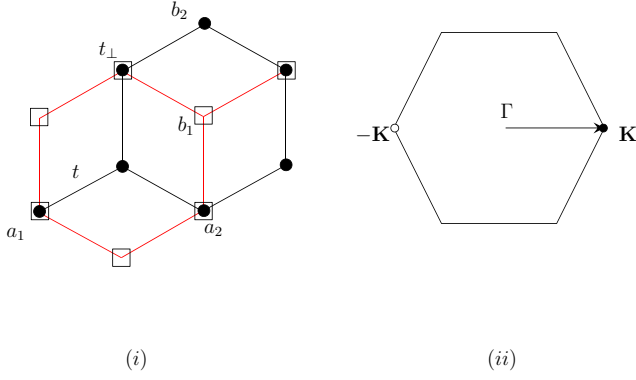


FIG. 3: (i) Illustration of the honeycomb bilayer lattice with only nearest-neighbor hopping terms. The squares represent the bottom layer, or layer 1, while the circles represent the top layer, or layer 2. The intralayer hopping is t , while the interlayer hopping is t_{\perp} . We label the dimerized sites as a_1 and a_2 , while the non-dimerized sites are labeled b_1 and b_2 . (ii) Illustration of the (reciprocal) \mathbf{k} space, with the parabolic degeneracy points $\mathbf{K} = \frac{4\pi}{3\sqrt{3}a}\hat{x}$ and $\mathbf{K}' = -\mathbf{K}$, where a is the (real-space) lattice constant, marked.

it only possesses two parabolic degeneracy points, rather than four Dirac cones. As stated earlier, this will make our system unstable to symmetry-breaking phases for arbitrarily weak interactions, thus justifying the use of perturbative RG methods. The Hamiltonian for this system is⁸

$$H = H_0^{\parallel} + H_0^{\perp} + H_I^{\parallel} + H_I^{\perp}, \quad (7)$$

where

$$H_0^{\parallel} = -t \sum_{\mathbf{R}, \delta} [b_1^{\dagger}(\mathbf{R} + \delta)a_1(\mathbf{R}) + b_2^{\dagger}(\mathbf{R} - \delta)a_2(\mathbf{R}) + \text{h.c.}], \quad (8)$$

$$H_0^{\perp} = -t_{\perp} \sum_{\mathbf{R}} [a_1^{\dagger}(\mathbf{R})a_2(\mathbf{R}) + \text{h.c.}], \quad (9)$$

$$\begin{aligned} H_I^{\parallel} &= \frac{1}{2} \sum_{k=1}^2 \sum_{\mathbf{R}\mathbf{R}'} V(\mathbf{R}' - \mathbf{R}) [n_{ak}(\mathbf{R}) - \frac{1}{2}] [n_{ak}(\mathbf{R}') - \frac{1}{2}] \\ &\quad + \sum_{k=1}^2 \sum_{\mathbf{R}\mathbf{R}'} V(\mathbf{R}' - \mathbf{R} + (-1)^{k-1}\delta) [n_{ak}(\mathbf{R}) - \frac{1}{2}] \\ &\quad \times [n_{bk}(\mathbf{R}' + (-1)^{k-1}\delta) - \frac{1}{2}] \\ &+ \frac{1}{2} \sum_{k=1}^2 \sum_{\mathbf{R}\mathbf{R}'} V(\mathbf{R}' - \mathbf{R} + (-1)^{k-1}\delta) [n_{bk}(\mathbf{R} + (-1)^{k-1}\delta) - \frac{1}{2}] \\ &\quad \times [n_{bk}(\mathbf{R}' + (-1)^{k-1}\delta) - \frac{1}{2}]. \end{aligned} \quad (10)$$

where $n_{ak}(\mathbf{R}) = a_k^{\dagger}(\mathbf{R})a_k(\mathbf{R})$, and similarly for $n_{bk}(\mathbf{R})$, and

$$H_I^{\perp} = \sum_{\mathbf{R}\mathbf{R}'} V_{\perp}(\mathbf{R} - \mathbf{R}') [n_{a1}(\mathbf{R}) - \frac{1}{2}] [n_{a2}(\mathbf{R}') - \frac{1}{2}]$$

$$\begin{aligned} &+ \sum_{\mathbf{R}\mathbf{R}'} V_{\perp}(\mathbf{R} - \mathbf{R}' + \delta) [n_{b1}(\mathbf{R} + \delta) - \frac{1}{2}] [n_{a2}(\mathbf{R}') - \frac{1}{2}] \\ &+ \sum_{\mathbf{R}\mathbf{R}'} V_{\perp}(\mathbf{R} - \mathbf{R}' + \delta) [n_{a1}(\mathbf{R}) - \frac{1}{2}] [n_{b2}(\mathbf{R}' - \delta) - \frac{1}{2}] \\ &+ \sum_{\mathbf{R}\mathbf{R}'} V_{\perp}(\mathbf{R} - \mathbf{R}' + 2\delta) [n_{b1}(\mathbf{R} + \delta) - \frac{1}{2}] [n_{b2}(\mathbf{R}' - \delta) - \frac{1}{2}]. \end{aligned} \quad (11)$$

Here, t and t_{\perp} are the intra-layer and inter-layer nearest-neighbor hopping integrals, respectively, δ is a vector that connects an a_1 site to a nearest-neighbor b_1 site, and $V(\mathbf{r})$ is an interaction that depends only on $|\mathbf{r}|$. The position vectors \mathbf{R} and \mathbf{R}' that we sum over are the positions of the dimerized sites. The three possible values of δ are $\frac{\sqrt{3}}{2}a\hat{x} + \frac{1}{2}a\hat{y}$, $-\frac{\sqrt{3}}{2}a\hat{x} + \frac{1}{2}a\hat{y}$, and $-a\hat{y}$. Whenever there is a sum on δ , we sum over all three vectors, while, if δ occurs without a sum over it, then we choose one such vector. For convenience, we introduced the notation $V_{\perp}(\mathbf{R}) = V(\mathbf{R} \pm c)$, where $2c$ is the distance between the two layers. We write the interaction terms in the form that we did because then the system represented by this Hamiltonian will be at half filling when the chemical potential is zero. We may show this as follows. Let us perform the following particle-hole transformation:

$$a_1(\mathbf{R}) = c_1^{\dagger}(\mathbf{R}), \quad (12)$$

$$a_2(\mathbf{R}) = -c_2^{\dagger}(\mathbf{R}), \quad (13)$$

$$b_1(\mathbf{R}) = -d_1^{\dagger}(\mathbf{R}), \quad (14)$$

$$b_2(\mathbf{R}) = d_2^{\dagger}(\mathbf{R}). \quad (15)$$

The hopping terms in our Hamiltonian become

$$\begin{aligned} H_0^{\parallel} &= t \sum_{\mathbf{R}, \delta} [d_1(\mathbf{R} + \delta)c_1^{\dagger}(\mathbf{R}) + d_2(\mathbf{R} - \delta)c_2^{\dagger}(\mathbf{R}) + \text{h.c.}] \\ &= -t \sum_{\mathbf{R}, \delta} [c_1^{\dagger}(\mathbf{R})d_1(\mathbf{R} + \delta) + c_2^{\dagger}(\mathbf{R})d_2(\mathbf{R} - \delta) \\ &\quad + \text{h.c.}] \end{aligned} \quad (16)$$

and

$$\begin{aligned} H_0^{\perp} &= t_{\perp} \sum_{\mathbf{R}} [c_1(\mathbf{R})c_2^{\dagger}(\mathbf{R}) + \text{h.c.}] \\ &= -t_{\perp} \sum_{\mathbf{R}} [c_2^{\dagger}(\mathbf{R})c_1(\mathbf{R}) \\ &\quad + \text{h.c.}]. \end{aligned} \quad (17)$$

We see that these terms have the same form as they originally did, but with a and b replaced by c and d , respectively. Now we will consider the interaction terms. We will consider, as an example, the following term from H_I^{\parallel} ,

$$[a_1^{\dagger}(\mathbf{R})a_1(\mathbf{R}) - \frac{1}{2}] [b_1^{\dagger}(\mathbf{R}' + \delta)b_1(\mathbf{R}' + \delta) - \frac{1}{2}]. \quad (18)$$

Performing the particle-hole transformation, this becomes

$$\begin{aligned} &[c_1(\mathbf{R})c_1^{\dagger}(\mathbf{R}) - \frac{1}{2}] [d_1(\mathbf{R}' + \delta)d_1^{\dagger}(\mathbf{R}' + \delta) - \frac{1}{2}] \\ &= [\frac{1}{2} - c_1^{\dagger}(\mathbf{R})c_1(\mathbf{R})] [\frac{1}{2} - d_1^{\dagger}(\mathbf{R}' + \delta)d_1(\mathbf{R}' + \delta)] \end{aligned}$$

$$= [c_1^\dagger(\mathbf{R})c_1(\mathbf{R}) - \frac{1}{2}][d_1^\dagger(\mathbf{R}' + \delta)d_1(\mathbf{R}' + \delta) - \frac{1}{2}]. \quad (19)$$

We see that, again, this term remains invariant in form, just as the hopping terms did. If we perform the same transformation on the rest of the interaction terms, we will find that they, too, are invariant. Therefore, the entire Hamiltonian is invariant under the above particle-hole transformation. Let us now find the average particle number per site.

$$\begin{aligned} \langle a_k^\dagger(\mathbf{R})a_k(\mathbf{R}) \rangle &= \langle c_k(\mathbf{R})c_k^\dagger(\mathbf{R}) \rangle \\ &= 1 - \langle c_k^\dagger(\mathbf{R})c_k(\mathbf{R}) \rangle. \end{aligned} \quad (20)$$

Since our Hamiltonian is invariant under the particle-hole transformation, $\langle a_k^\dagger(\mathbf{R})a_k(\mathbf{R}) \rangle = \langle c_k^\dagger(\mathbf{R})c_k(\mathbf{R}) \rangle$. Therefore,

$$\langle c_k^\dagger(\mathbf{R})c_k(\mathbf{R}) \rangle = 1 - \langle c_k^\dagger(\mathbf{R})c_k(\mathbf{R}) \rangle, \quad (21)$$

or $\langle c_k^\dagger(\mathbf{R})c_k(\mathbf{R}) \rangle = \frac{1}{2}$. The argument goes similarly for $\langle b_k^\dagger(\mathbf{R})b_k(\mathbf{R}) \rangle$. Therefore, since we may have up to one particle on a given site, we conclude that the system is at half filling.

B. Low-energy effective theory

We will now derive the low-energy effective theory associated with this Hamiltonian. Following the previous work⁶, we derive this theory by writing the partition function for the above theory in the form of a coherent-state path integral²¹ and integrating out the high-energy

modes, which correspond to the a_1 and a_2 sites. The result will be an effective action for the b_1 and b_2 sites. Throughout this work, we will be working at zero temperature. For the spinless case that we are currently considering, we will also set the on-site interaction $V(0) = 0$ for mathematical convenience, since it is impossible for two spinless fermions to occupy the same lattice point. The partition function associated with the above Hamiltonian is

$$Z = \int \mathcal{D}[a^*, a, b^*, b] e^{-S}, \quad (22)$$

where

$$\begin{aligned} S &= S_{0,a} + S_{0,b} + S_2 + S_4 \\ &= \int_0^\infty d\tau (\mathcal{L}_{0,a} + \mathcal{L}_{0,b} + \mathcal{L}_2 + \mathcal{L}_4), \end{aligned} \quad (23)$$

$$\mathcal{L}_{0,a} = \sum_{\mathbf{R}} \left[a^\dagger(\mathbf{R}, \tau) \left(\frac{\partial}{\partial \tau} + H_a - \mu \right) a(\mathbf{R}, \tau) \right], \quad (24)$$

$$\mathcal{L}_{0,b} = \sum_{\mathbf{R}} \left[b^\dagger(\mathbf{R}, \tau) \left(\frac{\partial}{\partial \tau} - \mu \right) b(\mathbf{R}, \tau) \right], \quad (25)$$

$$\mathcal{L}_2 = -t \sum_{\mathbf{R}, \delta} [b_1^*(\mathbf{R} + \delta, \tau)a_1(\mathbf{R}, \tau) + b_2^*(\mathbf{R} - \delta, \tau)a_2(\mathbf{R}, \tau) + \text{c.c.}], \quad (26)$$

$$\begin{aligned} \mathcal{L}_4 &= \frac{1}{2} \sum_{k=1}^2 \sum_{\mathbf{R}\mathbf{R}'} V(\mathbf{R}' - \mathbf{R}) [n_{ak}(\mathbf{R}, \tau)n_{ak}(\mathbf{R}', \tau) - n_{ak}(\mathbf{R}, \tau)] \\ &+ \sum_{k=1}^2 \sum_{\mathbf{R}\mathbf{R}'} V(\mathbf{R}' - \mathbf{R} + (-1)^{k-1}\delta) [n_{ak}(\mathbf{R}, \tau)n_{bk}(\mathbf{R}' + (-1)^{k-1}\delta) - \frac{1}{2}n_{ak}(\mathbf{R}, \tau) - \frac{1}{2}n_{bk}(\mathbf{R}' + (-1)^{k-1}\delta, \tau)] \\ &+ \frac{1}{2} \sum_{k=1}^2 \sum_{\mathbf{R}\mathbf{R}'} V(\mathbf{R}' - \mathbf{R}) [n_{bk}(\mathbf{R} + (-1)^{k-1}\delta, \tau)n_{bk}(\mathbf{R}' + (-1)^{k-1}\delta, \tau) - n_{bk}(\mathbf{R} + (-1)^{k-1}\delta, \tau)] \\ &+ \sum_{\mathbf{R}\mathbf{R}'} V_\perp(\mathbf{R}' - \mathbf{R}) [n_{a1}(\mathbf{R}, \tau)n_{a2}(\mathbf{R}', \tau) - \frac{1}{2}n_{a1}(\mathbf{R}, \tau) - \frac{1}{2}n_{a2}(\mathbf{R}', \tau)] \\ &+ \sum_{\mathbf{R}\mathbf{R}'} V_\perp(\mathbf{R}' - \mathbf{R} - \delta) [n_{b1}(\mathbf{R} + \delta, \tau)n_{a2}(\mathbf{R}', \tau) - \frac{1}{2}n_{b1}(\mathbf{R} + \delta, \tau) - \frac{1}{2}n_{a2}(\mathbf{R}', \tau)] \\ &+ \sum_{\mathbf{R}\mathbf{R}'} V_\perp(\mathbf{R}' - \mathbf{R} - \delta) [n_{a1}(\mathbf{R}, \tau)n_{b2}(\mathbf{R}' - \delta, \tau) - \frac{1}{2}n_{a1}(\mathbf{R}, \tau) - \frac{1}{2}n_{b2}(\mathbf{R}' - \delta, \tau)] \\ &+ \sum_{\mathbf{R}\mathbf{R}'} V_\perp(\mathbf{R}' - \mathbf{R} - 2\delta) [n_{b1}(\mathbf{R} + \delta, \tau)n_{b2}(\mathbf{R}' - \delta, \tau) - \frac{1}{2}n_{b1}(\mathbf{R} + \delta, \tau) - \frac{1}{2}n_{b2}(\mathbf{R}' - \delta, \tau)], \end{aligned} \quad (27)$$

and

$$H_a = \begin{bmatrix} 0 & -t_\perp \\ -t_\perp & 0 \end{bmatrix}. \quad (28)$$

Here, we define

$$a(\mathbf{R}, \tau) = \begin{bmatrix} a_1(\mathbf{R}, \tau) \\ a_2(\mathbf{R}, \tau) \end{bmatrix} \quad (29)$$

and similarly for $b(\mathbf{R}, \tau)$. We also define $n_{ak}(\mathbf{R}, \tau) = a_k^*(\mathbf{R}, \tau)a_k(\mathbf{R}, \tau)$, and similar expressions for b . From this point forward, we will set μ to zero so that our system is at half filling, as stated above.

We will now integrate out the a fields perturbatively. We do this by taking $S_{0,a}$ to be our “bare” action and performing a cumulant expansion to second order in the remaining part of the action. By doing this, we will have rewritten the partition function in the form,

$$Z = \int \mathcal{D}[b^*, b] \exp \left[- \int_0^\infty d\tau \mathcal{L}_{\text{eff}} \right], \quad (30)$$

where \mathcal{L}_{eff} is an effective Lagrangian containing only the b fields. We start by writing our partition function as

$$Z = Z_{0,a} \int \mathcal{D}[b^*, b] e^{-S_{0,b}} \langle e^{-S_2 - S_4} \rangle_{0,a}, \quad (31)$$

where $\langle \cdot \rangle_{0,a}$ is an average with respect to $S_{0,a}$ and

$$Z_{0,a} = \int \mathcal{D}[a^*, a] e^{-S_{0,a}}.$$

Note that we can factor out $e^{-S_{0,b}}$ because it does not contain any a fields. We will drop the factor of $Z_{0,a}$ from now on because it contributes a physically unimportant multiplicative constant to Z . We now perform the cumulant expansion,

$$\begin{aligned} \langle e^{-S_P} \rangle_{0,a} &= \exp \left[-\langle S_P \rangle_{0,a} + \frac{1}{2} (\langle S_P^2 \rangle_{0,a} - \langle S_P \rangle_{0,a}^2) + \dots \right] \\ &= \exp \left(-\langle S_P \rangle_{0,a} + \frac{1}{2} \langle S_P^2 \rangle_{0,a,C} + \dots \right), \end{aligned} \quad (32)$$

where $S_P = S_2 + S_4$ and a “ C ” in a subscript means to take a “connected” average; that is, only terms that are represented by connected Feynman diagrams contribute. In evaluating the first-order terms, we find the observation that $\langle n_{ak}(\mathbf{R}, \tau) \rangle_{0,a} = \frac{1}{2}$ to be useful; this comes from the fact that the system described by the action $S_{0,a}$ is at half filling when $\mu = 0$. Only terms in S_4 contribute to the first-order terms because each term in S_2 contains an odd number of a fields. The result that we obtain is

$$\begin{aligned} \langle S_P \rangle_{0,a} &= \frac{1}{2} \int_0^\beta d\tau \sum_{k=1}^2 \sum_{\mathbf{R}\mathbf{R}'} V(\mathbf{R}' - \mathbf{R}) [n_{bk}(\mathbf{R} + (-1)^{k-1}\delta, \tau) n_{bk}(\mathbf{R}' + (-1)^{k-1}\delta, \tau) - n_{bk}(\mathbf{R} + (-1)^{k-1}\delta, \tau)] \\ &+ \int_0^\beta d\tau \sum_{\mathbf{R}\mathbf{R}'} V_\perp(\mathbf{R}' - \mathbf{R} - 2\delta) [n_{b1}(\mathbf{R} + \delta, \tau) n_{b2}(\mathbf{R}' - \delta, \tau) - \frac{1}{2} n_{b1}(\mathbf{R} + \delta, \tau) - \frac{1}{2} n_{b2}(\mathbf{R}' - \delta, \tau)]. \end{aligned} \quad (33)$$

We see that the first-order term in the cumulant expansion only generates an interaction for the b fields. The kinetic term is generated by the second-order term. The only contribution to the kinetic term will come from $\langle S_2^2 \rangle_{0,a}$; all other terms are either zero, disconnected, or contribute to the interaction term. Upon introducing the Fourier transforms of the b fields with respect to imaginary time,

$$b_k(\mathbf{R}, \tau) = \frac{1}{\beta} \sum_{\omega} b_k(\mathbf{R}, \omega) e^{-i\omega\tau}, \quad (34)$$

where ω is a fermionic Matsubara frequency, and similarly for the Green’s functions $G_{ij}(\mathbf{R}, \tau)$, the term that we are considering becomes

$$\begin{aligned} \langle S_2^2 \rangle_{0,a} &= \frac{2t^2}{\beta} \sum_{\omega} \sum_{\mathbf{R}, \delta, \delta'} [G_{11}^a(\mathbf{R}, \omega) b_1^*(\mathbf{R} + \delta, \omega) b_1(\mathbf{R} + \delta', \omega) \\ &+ G_{12}^a(\mathbf{R}, \omega) b_1^*(\mathbf{R} + \delta, \omega) b_2(\mathbf{R} - \delta', \omega) \\ &+ G_{21}^a(\mathbf{R}, \omega) b_2^*(\mathbf{R} - \delta, \omega) b_1(\mathbf{R} + \delta', \omega) \\ &+ G_{22}^a(\mathbf{R}, \omega) b_2^*(\mathbf{R} - \delta, \omega) b_2(\mathbf{R} - \delta', \omega)]. \end{aligned} \quad (35)$$

For convenience, we are doing this calculation at finite temperature; we will take β to infinity at the end. We have made use of the fact that the Green’s functions for

the a fields are diagonal in position and spin space in writing the above. The Green’s functions are given by

$$G^a(\mathbf{R}, \omega) = (-i\omega + H_a)^{-1} = \frac{1}{\omega^2 + t_\perp^2} \begin{bmatrix} i\omega & -t_\perp \\ -t_\perp & i\omega \end{bmatrix}. \quad (36)$$

We now substitute this expression into $\langle S_2^2 \rangle_{0,a}$, but with ω set to zero. This is because, as is shown by one of us⁶, terms of higher order in ω are irrelevant under RG. The result is

$$\begin{aligned} \langle S_2^2 \rangle_{0,a} &= -\frac{2t^2}{\beta t_\perp} \sum_{\omega} \sum_{\mathbf{R}, \delta, \delta'} [b_1^*(\mathbf{R} + \delta, \omega) b_2(\mathbf{R} - \delta', \omega) \\ &+ b_2^*(\mathbf{R} - \delta, \omega) b_1(\mathbf{R} + \delta', \omega)]. \end{aligned} \quad (37)$$

If we rewrite this in terms of imaginary time and let the temperature go to zero, this becomes

$$\begin{aligned} \langle S_2^2 \rangle_{0,a} &= -\frac{2t^2}{t_\perp} \int_0^\infty d\tau \sum_{\mathbf{R}, \delta, \delta'} [b_1^*(\mathbf{R} + \delta, \tau) b_2(\mathbf{R} - \delta', \tau) \\ &+ b_2^*(\mathbf{R} - \delta, \tau) b_1(\mathbf{R} + \delta', \tau)]. \end{aligned} \quad (38)$$

Next, we consider second-order corrections to the interaction term. We will only go to this order in the interaction in the spinless case that we are currently considering; this is because, as shown in the previous work,

the lowest-order terms in the effective interaction for a nearest-neighbor interaction appear at second order in the cumulant expansion⁶. In the spin- $\frac{1}{2}$ case that we will consider later, we only need to retain first-order terms in the interaction because, for the on-site interaction considered in the previous work for that case, terms rep-

resenting the effective interaction appear at first order in the cumulant expansion⁶. The corrections that we wish to find are generated entirely by $\langle S_4^2 \rangle_{0,a,C}$; since all terms in $\langle S_2 S_4 \rangle_{0,a,C}$ contain odd powers of the a fields, it vanishes. We may employ Wick's theorem to evaluate $\langle S_4^2 \rangle_{0,a,C}$, obtaining, after considerable effort,

$$\langle S_4^2 \rangle_{0,a,C} = \frac{1}{4t_\perp} \int_0^\infty d\tau \sum_{\mathbf{R}} \left\{ \sum_{\mathbf{R}'} [\bar{V}(\mathbf{R}' - \mathbf{R} + \delta) n_{b1}(\mathbf{R}' + \delta, \tau) - \bar{V}(\mathbf{R}' - \mathbf{R} - \delta) n_{b2}(\mathbf{R}' - \delta, \tau)] \right\}^2, \quad (39)$$

where $\bar{V}(\mathbf{R}) = V(\mathbf{R}) - V_\perp(\mathbf{R})$. Putting all of our results together, we find that our effective Lagrangian is

$$\begin{aligned} \mathcal{L}_{\text{eff}} = & \sum_{\mathbf{R}} \left[b^\dagger(\mathbf{R}, \tau) \frac{\partial}{\partial \tau} b(\mathbf{R}, \tau) \right] + \frac{t^2}{t_\perp} \sum_{\mathbf{R}, \delta, \delta'} [b_1^*(\mathbf{R} + \delta, \tau) b_2(\mathbf{R} - \delta', \tau) + b_2^*(\mathbf{R} - \delta, \tau) b_1(\mathbf{R} + \delta', \tau)] \\ & + \frac{1}{2} \sum_{k=1}^2 \sum_{\mathbf{R}\mathbf{R}'} V(\mathbf{R}' - \mathbf{R}) [n_{bk}(\mathbf{R} + (-1)^{k-1} \delta, \tau) n_{bk}(\mathbf{R}' + (-1)^{k-1} \delta, \tau) - n_{bk}(\mathbf{R} + (-1)^{k-1} \delta, \tau)] \\ & + \sum_{\mathbf{R}\mathbf{R}'} V_\perp(\mathbf{R}' - \mathbf{R} - 2\delta) [n_{b1}(\mathbf{R} + \delta, \tau) n_{b2}(\mathbf{R}' - \delta, \tau) - \frac{1}{2} n_{b1}(\mathbf{R} + \delta, \tau) - \frac{1}{2} n_{b2}(\mathbf{R}' - \delta, \tau)] \\ & - \frac{1}{8t_\perp} \sum_{\mathbf{R}} \left\{ \sum_{\mathbf{R}'} [\bar{V}(\mathbf{R}' - \mathbf{R} + \delta) n_{b1}(\mathbf{R}' + \delta, \tau) - \bar{V}(\mathbf{R}' - \mathbf{R} - \delta) n_{b2}(\mathbf{R}' - \delta, \tau)] \right\}^2. \end{aligned} \quad (40)$$

We now wish to write a theory for modes near the parabolic degeneracy points. To do this, we first perform a Fourier transform of the fields with respect to position:

$$b_{i\sigma}(\mathbf{R}, \tau) = \frac{1}{\sqrt{N}} \sum_{\mathbf{k}} b_{i\sigma}(\mathbf{k}, \tau), \quad (41)$$

where N is the number of unit cells in our system. Let us first consider the tight-binding term. If we substitute the above Fourier transform into that term, it becomes

$$\frac{t^2}{t_\perp} \sum_{\mathbf{k}} [(d^*(\mathbf{k}))^2 b_1^*(\mathbf{k}, \tau) b_2(\mathbf{k}, \tau) + (d(\mathbf{k}))^2 b_2^*(\mathbf{k}, \tau) b_1(\mathbf{k}, \tau)], \quad (42)$$

where

$$d(\mathbf{k}) = \sum_{\delta} e^{i\mathbf{k} \cdot \delta} = 2e^{-ik_y a/2} \cos\left(\frac{\sqrt{3}}{2} k_x a\right) + e^{ik_y a}. \quad (43)$$

We will now expand $(d(\pm\mathbf{K} + \mathbf{q}))^2$, where $\pm\mathbf{K} = \pm\frac{4\pi}{3\sqrt{3}a}\hat{\mathbf{x}}$ are the parabolic degeneracy points, to second order in \mathbf{q} ; all higher order terms are irrelevant under RG⁶. The result is

$$(d(\pm\mathbf{K} + \mathbf{q}))^2 \approx \frac{(q_x \mp iq_y)^2}{2m}, \quad (44)$$

where the effective mass m is given by

$$m = \frac{2t_\perp}{9a^2 t^2}. \quad (45)$$

We may therefore write our theory in terms of the four-component field,

$$\psi(\mathbf{q}, \tau) = \begin{bmatrix} b_1(\mathbf{K} + \mathbf{q}, \tau) \\ b_2(\mathbf{K} + \mathbf{q}, \tau) \\ b_1(-\mathbf{K} + \mathbf{q}, \tau) \\ b_2(-\mathbf{K} + \mathbf{q}, \tau) \end{bmatrix}. \quad (46)$$

In particular, we will be rewriting the theory to include only modes near the parabolic degeneracy points. In other words, we are imposing a low-energy cutoff of the type introduced in RG calculations, which we are interested in performing. The non-interacting part of the effective Lagrangian \mathcal{L}_0 becomes

$$\mathcal{L}_0 = \sum_{\mathbf{q}} \left[\psi^\dagger(\mathbf{q}, \tau) \left(\frac{\partial}{\partial \tau} + \sum_{a=x,y} \Sigma^a d^a(\mathbf{q}) \right) \psi(\mathbf{q}, \tau) \right], \quad (47)$$

where

$$d^x(\mathbf{q}) = \frac{q_x^2 - q_y^2}{2m}, \quad d^y(\mathbf{q}) = \frac{q_x q_y}{m}, \quad (48)$$

$\Sigma^x = 1_2 \sigma^x = \gamma_2$ and $\Sigma^y = \tau^z \sigma^y = \gamma_1$. The τ matrices in the latter two definitions are Pauli matrices acting in the valley ($\pm\mathbf{K}$) space, while the σ matrices act in layer (1, 2) space. We also write the Σ matrices in terms of the Dirac γ matrices used often in the literature. We now rewrite the above Lagrangian in position space in

the continuum approximation, obtaining

$$\mathcal{L}_0 = \frac{1}{A_{uc}} \int d^2\mathbf{r} \left[\psi^\dagger(\mathbf{r}, \tau) \left(\frac{\partial}{\partial \tau} + \sum_{a=x,y} \Sigma^a d^a(\mathbf{p}) \right) \psi(\mathbf{r}, \tau) \right], \quad (49)$$

where A_{uc} is the area of a unit cell. This theory will serve as the Gaussian fixed point for our RG calculations.

We now turn our attention to the interaction terms. The general procedure that we will follow is to perform a Fourier transform of the interactions $V(\mathbf{r})$ and $V_\perp(\mathbf{r})$ and of the ‘‘particle number’’ fields $n_{bk}(\mathbf{r}, \tau)$, as follows:

$$V(\mathbf{r}) = \frac{1}{\sqrt{N}} \sum_{\mathbf{q}} V(\mathbf{q}) e^{i\mathbf{q}\cdot\mathbf{r}}, \quad (50)$$

and similarly for $V_\perp(\mathbf{r})$ and $n_{bk}(\mathbf{r}, \tau)$. We then drop all but the constant term of V in the momentum, since all higher-order terms are irrelevant under RG⁶. We will also find it useful to express $n_{bk}(\mathbf{q}, \tau)$ in terms of the b fields:

$$n_{bk}(\mathbf{q}, \tau) = \frac{1}{\sqrt{N}} \sum_{\mathbf{k}, \mathbf{G}} b_{k\sigma}^*(\mathbf{k}, \tau) b_{k\sigma}(\mathbf{k} + \mathbf{q} + \mathbf{G}, \tau), \quad (51)$$

where \mathbf{G} is a reciprocal lattice vector. We will illustrate this procedure using the inter-layer part of the interaction. We will begin with the quartic term,

$$\sum_{\mathbf{R}, \mathbf{R}'} V_\perp(\mathbf{R} - \mathbf{R}' + 2\delta) n_{b1}(\mathbf{R} + \delta, \tau) n_{b2}(\mathbf{R}' - \delta, \tau). \quad (52)$$

In this case, we will define

$$V_{\perp, \delta}(\mathbf{r}) = V_\perp(\mathbf{r} + \delta), \quad (53)$$

as well as its Fourier transform,

$$V_{\perp, \delta}(\mathbf{r}) = \frac{1}{\sqrt{N}} \sum_{\mathbf{q}} V_{\perp, \delta}(\mathbf{q}) e^{i\mathbf{q}\cdot(\mathbf{R} + \delta)}. \quad (54)$$

Since the above expression for the quartic interaction does not depend on which choice of δ we make, we may just as well rewrite it in terms of a sum over all three vectors:

$$\frac{1}{3} \sum_{\delta} \sum_{\mathbf{R}, \mathbf{R}'} V_\perp(\mathbf{R} - \mathbf{R}' + 2\delta) n_{b1}(\mathbf{R} + \delta, \tau) n_{b2}(\mathbf{R}' - \delta, \tau) \quad (55)$$

If we now perform the appropriate Fourier transforms and evaluate the sums over \mathbf{R} and \mathbf{R}' , we obtain

$$\frac{1}{3} \sqrt{N} \sum_{\mathbf{q}} \left[\sum_{\delta} V_{\perp, -\delta}(\mathbf{q}) \right] n_{b1}(-\mathbf{q}, \tau) n_{b2}(\mathbf{q}, \tau). \quad (56)$$

We will now impose a low-energy cutoff, as we did for the ‘‘bare’’ action; that is, we only keep modes with momenta near $\pm\mathbf{K}$. In Equation (51), we may impose this cutoff by restricting \mathbf{q} so that both \mathbf{k} and $\mathbf{k} + \mathbf{q} + \mathbf{G}$ are close to a parabolic degeneracy point. This is possible if \mathbf{q} is close to 0 or $\pm 2\mathbf{K}$. For each of these cases, Equation (51) becomes, in terms of the field $\psi(\mathbf{k}, \tau)$ introduced above,

$$n_{bk}(\mathbf{q}, \tau) \approx \frac{1}{\sqrt{N}} \sum_{\mathbf{k}, \mathbf{G}} \psi^\dagger(\mathbf{k}, \tau) M_k^{(f)} \psi(\mathbf{k} + \mathbf{q} + \mathbf{G}, \tau), \quad (57)$$

$$n_{bk}(2\mathbf{K} + \mathbf{q}, \tau) \approx \frac{1}{\sqrt{N}} \sum_{\mathbf{k}, \mathbf{G}} \psi^\dagger(\mathbf{k}, \tau) (M_k^{(b)})^T \psi(\mathbf{k} + \mathbf{q} + \mathbf{G}, \tau), \quad (58)$$

and

$$n_{bk}(-2\mathbf{K} + \mathbf{q}, \tau) \approx \frac{1}{\sqrt{N}} \sum_{\mathbf{k}, \mathbf{G}} \psi^\dagger(\mathbf{k}, \tau) M_k^{(b)} \psi(\mathbf{k} + \mathbf{q} + \mathbf{G}, \tau), \quad (59)$$

where the matrices $M_k^{(f)}$ and $M_k^{(b)}$ are defined in the previous work⁶; we repeat their definitions here for convenience:

$$M_1^{(f)} = \begin{bmatrix} 1 & 0 & 0 & 0 \\ 0 & 0 & 0 & 0 \\ 0 & 0 & 1 & 0 \\ 0 & 0 & 0 & 0 \end{bmatrix}, \quad M_2^{(f)} = \begin{bmatrix} 0 & 0 & 0 & 0 \\ 0 & 1 & 0 & 0 \\ 0 & 0 & 0 & 0 \\ 0 & 0 & 0 & 1 \end{bmatrix} \quad (60)$$

$$M_1^{(b)} = \begin{bmatrix} 0 & 0 & 1 & 0 \\ 0 & 0 & 0 & 0 \\ 0 & 0 & 0 & 0 \\ 0 & 0 & 0 & 0 \end{bmatrix}, \quad M_2^{(b)} = \begin{bmatrix} 0 & 0 & 0 & 0 \\ 0 & 0 & 0 & 1 \\ 0 & 0 & 0 & 0 \\ 0 & 0 & 0 & 0 \end{bmatrix} \quad (61)$$

We now take our quartic term and expand the potential around each of the above points. We only keep the constant term since all higher-order terms are irrelevant under RG⁶. Doing this and using Equations (57)–(59), we obtain

$$\begin{aligned} & \sum_{\mathbf{R}} [V_{\perp, N, 0} (\psi^\dagger M_1^{(f)} \psi) (\psi^\dagger M_2^{(f)} \psi) (\mathbf{R}, \tau) \\ & + V_{\perp, N, K} (\psi^\dagger M_1^{(b)} \psi) (\psi^\dagger (M_2^{(b)})^T \psi) (\mathbf{R}, \tau) \\ & + V_{\perp, N, K}^* (\psi^\dagger (M_1^{(b)})^T \psi) (\psi^\dagger M_2^{(b)} \psi) (\mathbf{R}, \tau), \end{aligned} \quad (62)$$

where

$$V_{\perp, N, 0} = \frac{1}{3} \sum_{\mathbf{R}, \delta} V_\perp(\mathbf{R} - \delta) \quad (63)$$

and

$$V_{\perp, N, K} = \frac{1}{3} \sum_{\mathbf{R}, \delta} V_\perp(\mathbf{R} - \delta) e^{2i\mathbf{K}\cdot(\mathbf{R} - \delta)}. \quad (64)$$

It can be shown that $V_{\perp, N, K}$ is zero due to the symmetry of the honeycomb lattice that the b sites form. Our quartic term is then just

$$V_{\perp, N, 0} \sum_{\mathbf{R}} (\psi^\dagger M_1^{(f)} \psi) (\psi^\dagger M_2^{(f)} \psi) (\mathbf{R}, \tau), \quad (65)$$

or, in the continuum approximation,

$$\frac{V_{\perp, N, 0}}{A_{uc}} \int d^2\mathbf{R} (\psi^\dagger M_1^{(f)} \psi) (\psi^\dagger M_2^{(f)} \psi) (\mathbf{R}, \tau). \quad (66)$$

Performing this procedure on all terms in the Lagrangian, we finally arrive at our effective low-energy theory,

$$\begin{aligned}
\mathcal{L}_{\text{eff}} = & \frac{1}{A_{uc}} \int d^2\mathbf{R} \psi^\dagger \left[\frac{\partial}{\partial\tau} + H(\mathbf{p}) \right] \psi \\
& + \frac{1}{2A_{uc}} \int d^2\mathbf{R} \sum_{k=1}^2 \{ V_0 (\psi^\dagger M_k^{(f)} \psi)^2 + V_K [(\psi^\dagger [M_k^{(b)}]^T \psi) (\psi^\dagger M_k^{(b)} \psi) + (\psi^\dagger M_k^{(b)} \psi) (\psi^\dagger [M_k^{(b)}]^T \psi)] \} \\
& + \frac{V_{\perp,N}}{A_{uc}} \int d^2\mathbf{R} (\psi^\dagger M_1^{(f)} \psi) (\psi^\dagger M_2^{(f)} \psi) - \frac{(V_{0,N} - V_{\perp,N})^2}{8t_{\perp} A_{uc}} \int d^2\mathbf{R} (\psi^\dagger [M_1^{(f)} - M_2^{(f)}] \psi) (\psi^\dagger [M_1^{(f)} - M_2^{(f)}] \psi) \\
& - \mu' \int d^2\mathbf{R} \psi^\dagger \psi,
\end{aligned} \tag{67}$$

where

$$V_0 = \sum_{\mathbf{R}} V(\mathbf{R}) \tag{68}$$

$$V_K = \sum_{\mathbf{R}} V(\mathbf{R}) \cos(2\mathbf{K} \cdot \mathbf{R}) \tag{69}$$

$$V_{0,N} = \frac{1}{3} \sum_{\mathbf{R},\delta} V(\mathbf{R} - \delta) \tag{70}$$

$$V_{\perp,N} = \frac{1}{3} \sum_{\mathbf{R},\delta} V_{\perp}(\mathbf{R} - \delta) \tag{71}$$

There are two things to note about this expression. First of all, we have what appear to be “mixed” terms in the Lagrangian; in other words, terms of the form, $(\psi^\dagger A \psi)(\psi^\dagger B \psi)$, where A and B are two different matrices. However, as we will see shortly, we can rewrite the Lagrangian in a form that does not have such “mixed” terms present; something similar appears in Ref.⁶. Second of all is the quadratic, chemical potential-like, term. We may think of the undetermined constant μ' as being chosen in such a way as to cancel out the quadratic terms that are generated from the quartic terms under RG. We require that this occur because we know that our original lattice model and, in fact, the model that we obtain after integrating out the “dimerized” sites, are at half filling (that is, they possess particle-hole symmetry), and therefore this should be reflected in our effective low-energy theory as well. We may accomplish this by writing a Hamiltonian corresponding to the above action, performing the particle-hole transformation, $\psi \rightarrow -\tau_1 \sigma_3 \psi^*$, and finding what value of μ' would leave the Hamiltonian invariant under this transformation.

We could, in principle, have also determined the value of μ' when we wrote down the above effective low-energy theory. Strictly speaking, we should not simply drop all of the modes above the cutoff, as we did here, but rather integrate them out in a perturbative scheme similar to what is done in an RG analysis. This, at first order, will not change our quartic terms because it only generates the tree-level quartic terms. However, it will generate both tree-level and one-loop contributions to the quadratic terms. It would, however, be somewhat cumbersome, and given the above particle-hole symmetry arguments equally unnecessary, to determine these

one-loop contributions to the chemical potential.

C. Renormalization group analysis of the theory

We are now ready to perform the RG analysis of the above low-energy theory. Before we begin this analysis, however, we note that, as shown by one of us⁶, there are four independent coupling constants in our theory due to symmetries of the underlying honeycomb bilayer lattice and Fierz identities; we would therefore like to rewrite the theory in terms of four such coupling constants. Following the previous work⁶, we choose to rewrite the interaction terms in the form,

$$\begin{aligned}
\frac{1}{2} \int d^2\mathbf{R} \{ & g_{A_1} (\psi^\dagger A_1 \psi)^2 + g_{A_2} [(\psi^\dagger A_2 \psi)^2 + (\psi^\dagger D_1 \psi)^2] \\
& + g_{D_2} (\psi^\dagger D_2 \psi)^2 + g_{\gamma} [(\psi^\dagger C_3 \psi)^2 + (\psi^\dagger D_3 \psi)^2] \} \tag{72}
\end{aligned}$$

where the A , B , C , and D matrices are defined as follows⁶:

$$A = \{1_2, 1_2 \sigma^x, \tau^x \sigma^x, \tau^x 1_2\} \tag{73}$$

$$B = \{\tau^z \sigma^x, \tau^z 1_2, \tau^y \sigma^x, -\tau^y 1_2\} \tag{74}$$

$$C = \{1_2 \sigma^z, -1_2 \sigma^y, \tau^x \sigma^y, -\tau^x \sigma^z\} \tag{75}$$

$$D = \{\tau^z \sigma^y, \tau^z \sigma^z, \tau^y \sigma^y, -\tau^y \sigma^z\} \tag{76}$$

We may use the Fierz identities stated in the previous work⁶ to rewrite our theory in the above form, in which case the coupling constants are

$$g_{A_1} = \frac{1}{2A_{uc}} \left[2V_{\perp,N} + \frac{(V_{0,N} - V_{\perp,N})^2}{2t_{\perp}} \right], \tag{77}$$

$$g_{A_2} = \frac{1}{2A_{uc}} \left[V_0 - V_{\perp,N} - V_K - \frac{(V_{0,N} - V_{\perp,N})^2}{2t_{\perp}} \right] \tag{78}$$

$$g_{D_2} = -2g_{A_2}, \tag{79}$$

$$g_{\gamma} = -g_{A_2}. \tag{80}$$

These will be the initial conditions that we will use for the flow equations derived by one of us for spinless fermions⁶. These initial conditions will depend on the form of the interaction $V(\mathbf{R})$ that we choose. We will consider two forms for this interaction. First will be a simple exponential model,

$$V(\mathbf{R}) = U_0 e^{-\pi|\mathbf{R}|/\xi}. \tag{81}$$

Second will be a screened Coulomb-like interaction, with the screening being due to two infinite planar conducting plates, between which the charge is located. We consider this second case because of experiments with gated bilayer graphene, such as the experiments in Refs.^{3,4}; in these cases, the gates will serve as the conducting plates. We will assume that the distance between the plates is much larger than the distance between the two layers so that we may assume that the particles are exactly halfway between the two plates. If the distance between the plates is ξ , then the interaction is given by

$$V(\mathbf{R}) = U_0 \sum_{n=-\infty}^{\infty} \frac{1}{|\mathbf{R}/\xi + n\hat{\mathbf{z}}|}. \quad (82)$$

In both cases, U_0 is a sufficiently small constant, so that our system will be at weak coupling. Also note that the length scale, ξ , sets the range of the interaction in both cases. In the second case, we find that, for $|\mathbf{R}| \gg \xi$, we may approximate the sum as

$$V(\mathbf{R}) \approx U_0 \frac{2\sqrt{2}e^{-\pi|\mathbf{R}|/\xi}}{\sqrt{|\mathbf{R}|/\xi}}. \quad (83)$$

We will show that this is, indeed, the long-distance behavior of the interaction in the appendix. In the opposite limit, $|\mathbf{R}| \ll \xi$, we simply approximate the interaction with the first few terms of the sum around $n = 0$. In order to compare our results to those from the previous work for the case of a nearest-neighbor interaction⁶, we will add a nearest-neighbor interaction U_{NN} on top of these finite-range interactions. We do this because, as $\xi \rightarrow 0$, both forms of the interaction, Equations (81) and (82), go to zero at all lattice points except for $\mathbf{R} = 0$. Since we are dealing with spinless fermions, taking ξ to zero would therefore effectively eliminate the interaction altogether. By adding this additional nearest-neighbor interaction, we will be able to recover the results found in the previous work in the limit of short-ranged interactions⁶. We only do this for the spinless case because, in the spin- $\frac{1}{2}$ case that we will discuss later, the case considered in the previous work⁶ that we wish for our problem to reduce to in the short-range limit is that of an on-site interaction, rather than a nearest-neighbor interaction.

Using these expressions, we may find the initial coupling constants given above for various values of ξ . We may then determine the flows of said constants using the RG equations derived by one of us⁶, which we will repeat here for convenience:

$$\frac{dg_{A_1}}{d \ln s} = -4g_{A_1}g_{A_2} \frac{mA_{uc}^2}{4\pi} \quad (84)$$

$$\begin{aligned} \frac{dg_{A_2}}{d \ln s} &= -(g_{A_1}^2 - 2g_{A_1}g_{A_2} + 8g_{A_2}^2 - 2g_{A_2}g_{D_2} + g_{D_2}^2 \\ &\quad + 4(3g_{A_2} - g_{D_2})g_\gamma + 6g_\gamma^2) \frac{mA_{uc}^2}{4\pi} \end{aligned} \quad (85)$$

$$\frac{dg_{D_2}}{d \ln s} = 2(2g_{A_2}^2 + 2g_{A_1}g_{D_2} - 6g_{A_2}g_{D_2} - 2g_{D_2}^2$$

$$+ 8g_{A_2}g_\gamma + 2g_\gamma^2) \frac{mA_{uc}^2}{4\pi} \quad (86)$$

$$\frac{dg_\gamma}{d \ln s} = -2g_\gamma(-2g_{A_1} + 2g_{A_2} + 2g_\gamma) \frac{mA_{uc}^2}{4\pi} \quad (87)$$

Note that the multiplicative constants differ from those in the original equations; this is because we use a different scale for the fields (in the original work, there was no factor of $\frac{1}{A_{uc}}$ in the ‘‘bare’’ action⁶). We will find it convenient to work in terms of the dimensionless coupling constants,

$$g' = \frac{mA_{uc}^2}{4\pi} g. \quad (88)$$

In this case, the multiplicative constant $\frac{mA_{uc}^2}{4\pi}$ is removed from the right-hand sides of the above flow equations. Another property of these equations that we will make use of is the fact that they are invariant under the following rescaling:

$$g \rightarrow \alpha g, \ln s \rightarrow \frac{\ln s}{\alpha} \quad (89)$$

This means that, if we apply this rescaling to any solution of the flow equations, then we obtain another solution. This implies that, if we rescale the initial conditions for the flow, then there will be no qualitative changes to said flow; they are simply ‘‘stretched’’, much like a rubber sheet.

In order to determine which phase our system will go into, we must now consider the flow of the susceptibilities to forming different orders. To find these susceptibilities, we first introduce source terms representing each possible order parameter; the additional terms that we introduce into the Lagrangian are

$$\begin{aligned} \mathcal{L}_{\text{source}} &= \sum_i \frac{\Delta_{ph}^{\mathcal{O}_i}}{A_{uc}} \int d^2\mathbf{R} \psi^\dagger \mathcal{O}_i \psi(\mathbf{R}, \tau) \\ &\quad + \sum_i \frac{\Delta_{pp}^{\mathcal{O}_i}}{A_{uc}} \int d^2\mathbf{R} \psi_a \mathcal{O}_{i,ab} \psi_b(\mathbf{R}, \tau) + \text{c.c.} \end{aligned} \quad (90)$$

where \mathcal{O}_i runs over all SU(4) generators. We then find the flows of the constants $\Delta_{ph}^{\mathcal{O}_i}$ and $\Delta_{pp}^{\mathcal{O}_i}$ under our RG transformation and determine which diverges fastest as we increase s . This procedure has been done by one of us⁶, and the result is that all of the order parameters $\Delta_{ph}^{\mathcal{O}_i}$ and $\Delta_{pp}^{\mathcal{O}_i}$ have flow equations of the form

$$\frac{d \ln \Delta}{d \ln s} = 2 + \sum_M C_M g_M \frac{mA_{uc}^2}{4\pi}, \quad (91)$$

where M runs over all unique couplings in our theory (A_1 , A_2 , D_2 , and γ), and the C_M are constants that depend on the order parameter Δ being considered. The values of these coefficients are listed in Table I and Equations (84)–(87) of Ref.⁶. The second term on the right-hand side of the above equation is the susceptibility.

D. Determination of Phases

We are now ready to determine which phase we enter for an interaction with a given range. First, we must find the initial coupling constants g_{A_1} , g_{A_2} , g_{D_2} , and g_γ from Equations (77)–(80) for various values of the interaction range d for both of the above interaction forms, as given in Equations (81) and (82). Next, we find the ratios,

$$\left(\frac{g_{A_1}}{g_{A_2}}, \frac{g_{D_2}}{g_{A_2}}, \frac{g_\gamma}{g_{A_2}} \right) = \left(\frac{g'_{A_1}}{g'_{A_2}}, \frac{g'_{D_2}}{g'_{A_2}}, \frac{g'_\gamma}{g'_{A_2}} \right),$$

and multiply each ratio by a small value of the dimensionless coupling g'_{A_2} , thus obtaining a complete set of initial dimensionless couplings g'_{A_1} , g'_{A_2} , g'_{D_2} , and g'_γ . We then solve the flow equations for these couplings and use them to determine the susceptibilities to all of the different orders that we determined above. Due to the scaling property mentioned earlier, we may choose any sufficiently small value of g'_{A_2} and the relative magnitudes of the susceptibilities will remain the same; that is, this rescaling will not change which phase we predict. When the coupling constants diverge, we will find that the above ratios approach finite values. These fixed ratios have been found by one of us⁶, and, if $g_{A_2} < 0$, two of these fixed points are stable in that, if we perturb the ratios slightly, then we will flow back to the original fixed points. The first of these two points is

$$\left(\frac{g_{A_1}}{g_{A_2}}, \frac{g_{D_2}}{g_{A_2}}, \frac{g_\gamma}{g_{A_2}} \right) = (0, 6.519, 0), \quad (92)$$

which is found to correspond a quantum anomalous Hall phase, or a finite expectation value of $D_2 = i\gamma_1\gamma_2 = \tau^z\sigma^z$. The other stable fixed point is

$$\left(\frac{g_{A_1}}{g_{A_2}}, \frac{g_{D_2}}{g_{A_2}}, \frac{g_\gamma}{g_{A_2}} \right) = (0, -1.085, 0). \quad (93)$$

At this fixed point, we find two competing phases⁶ — an inversion symmetry-breaking phase in which there is an imbalance in the amount of charge on one layer with respect to the other (hereafter referred to as the “layer-polarized phase”), or a finite expectation value of $C_1 = \gamma_0 = 1_2\sigma^z$, and a Kekulé phase with finite expectation values of $C_3 = \gamma_3 = \tau^x\sigma^y$ and $D_3 = \gamma_5 = \tau^y\sigma^y$. In this case, we must look at the susceptibilities just before we reach the fixed point in order to determine which of these phases we are entering⁶. We presented the generic phase diagram for spinless fermions in Figure 1.

For our calculation, we chose to set $U_0 = \frac{e^2}{10,000d}$, where $e = 4.808 \times 10^{-10}$ esu is the charge of an electron and $d = 3.7$ Å is the spacing between two layers in graphite²²; in other words, we are using a heavily screened Coulomb interaction. We also used the hopping parameters for graphite²³; that is, $t = 3.12$ eV and $t_\perp = 0.377$ eV. We also set the additional nearest-neighbor interaction to $U_{NN} = 0.02U_0$.

We find that, for the screened Coulomb-like interaction, the system experiences three phase transitions as we increase the range of the interaction. When $\xi < 0.396a$, we find the layer-polarized phase, in agreement with the previous work⁶. For $0.396a < \xi < 21.05a$, we find the quantum anomalous Hall phase. For $21.05a < \xi < 119.73a$, we obtain the Kekulé phase. Finally, for $\xi > 119.73a$, we go back into the layer-polarized phase.

In the case of the exponential interaction, on the other hand, we only see two phase transitions. The phases that we see are the same as the first three in the case of the screened Coulomb-like interaction, with the transition from the layer-polarized phase to the quantum anomalous Hall phase occurring at $\xi = 0.392a$ and that from the quantum anomalous Hall phase to the Kekulé phase occurring at $\xi = 12.01a$. We suspect that there should be a third transition from the Kekulé phase back to the layer-polarized phase for some value of $\xi > 800a$.

III. SPIN- $\frac{1}{2}$ CASE

A. Starting Hamiltonian

We now consider the spin- $\frac{1}{2}$ case. As before, we will consider a tight-binding honeycomb bilayer with only nearest-neighbor hopping and a two-particle interaction. The Hamiltonian is

$$H = H_0^\parallel + H_0^\perp + H_I^\parallel + H_I^\perp, \quad (94)$$

where

$$H_0^\parallel = -t \sum_{\mathbf{R}, \delta, \sigma} [b_{1\sigma}^\dagger(\mathbf{R}+\delta)a_{1\sigma}(\mathbf{R}) + b_{2\sigma}^\dagger(\mathbf{R}-\delta)a_{2\sigma}(\mathbf{R}) + \text{h.c.}], \quad (95)$$

$$H_0^\perp = -t_\perp \sum_{\mathbf{R}, \sigma} [a_{1\sigma}^\dagger(\mathbf{R})a_{2\sigma}(\mathbf{R}) + \text{h.c.}], \quad (96)$$

$$\begin{aligned} H_I^\parallel = & \sum_{\mathbf{R}\mathbf{R}'} V(\mathbf{R} - \mathbf{R}' + \delta) [n_{a1}(\mathbf{R}) - 1] [n_{b1}(\mathbf{R}' + \delta) - 1] \\ & + \sum_{\mathbf{R}\mathbf{R}'} V(\mathbf{R} - \mathbf{R}' - \delta) [n_{a2}(\mathbf{R}) - 1] [n_{b2}(\mathbf{R}' - \delta) - 1] \\ & + \frac{1}{2} \sum_k \sum_{\mathbf{R} \neq \mathbf{R}'} V(\mathbf{R} - \mathbf{R}') [n_{ak}(\mathbf{R}) - 1] [n_{ak}(\mathbf{R}') - 1] \\ & + V(0) \sum_k \sum_{\mathbf{R}} [n_{ak\uparrow}(\mathbf{R}) - \frac{1}{2}] [n_{ak\downarrow}(\mathbf{R}) - \frac{1}{2}] \\ & + \frac{1}{2} \sum_k \sum_{\mathbf{R} \neq \mathbf{R}'} V(\mathbf{R} - \mathbf{R}') [n_{bk}(\mathbf{R} + (-1)^{k-1}\delta) - 1] \\ & \times [n_{bk}(\mathbf{R}' + (-1)^{k-1}\delta) - 1] \\ & + V(0) \sum_k \sum_{\mathbf{R}} [n_{bk\uparrow}(\mathbf{R} + (-1)^{k-1}\delta) - \frac{1}{2}] \\ & \times [n_{bk\downarrow}(\mathbf{R} + (-1)^{k-1}\delta) - \frac{1}{2}], \end{aligned} \quad (97)$$

and

$$H_I^\perp = \sum_{\mathbf{R}\mathbf{R}'} V_\perp(\mathbf{R} - \mathbf{R}') [n_{a1}(\mathbf{R}) - 1] [n_{a2}(\mathbf{R}') - 1]$$

$$\begin{aligned}
& + \sum_{\mathbf{R}\mathbf{R}'} V_{\perp}(\mathbf{R} - \mathbf{R}' + \delta)[n_{b1}(\mathbf{R} + \delta) - 1][n_{a2}(\mathbf{R}') - 1] \\
& + \sum_{\mathbf{R}\mathbf{R}'} V_{\perp}(\mathbf{R} - \mathbf{R}' + \delta)[n_{a1}(\mathbf{R}) - 1][n_{b2}(\mathbf{R}' - \delta) - 1] \\
& + \sum_{\mathbf{R}\mathbf{R}'} V_{\perp}(\mathbf{R} - \mathbf{R}' + 2\delta)[n_{b1}(\mathbf{R} + \delta) - 1] \\
& \times [n_{b2}(\mathbf{R}' - \delta) - 1], \tag{98}
\end{aligned}$$

where $n_{ak}(\mathbf{R}) = \sum_{\sigma} a_{k\sigma}^{\dagger}(\mathbf{R})a_{k\sigma}(\mathbf{R})$, and similarly for $n_{bk}(\mathbf{R})$. Aside from the introduction of the spin index for the creation and annihilation operators, all of our notation here is the same as in the spinless case. Again, we write the interaction term in this form so that the system represented by this Hamiltonian will be at half filling when the chemical potential is zero. We may show this in a similar manner as before using the following particle-hole transformation:

$$a_{1\sigma}(\mathbf{R}) = c_{1\sigma}^{\dagger}(\mathbf{R}), \tag{99}$$

$$a_{2\sigma}(\mathbf{R}) = -c_{2\sigma}^{\dagger}(\mathbf{R}), \tag{100}$$

$$b_{1\sigma}(\mathbf{R}) = -d_{1\sigma}^{\dagger}(\mathbf{R}), \tag{101}$$

$$b_{2\sigma}(\mathbf{R}) = d_{2\sigma}^{\dagger}(\mathbf{R}). \tag{102}$$

B. Low-energy effective theory

As before, our next step is to derive the low-energy effective theory for the above Hamiltonian by writing the

partition function associated with it as a coherent-state path integral and integrating out the high-energy modes. The partition function associated with the above Hamiltonian is

$$Z = \int \mathcal{D}[a^*, a, b^*, b] e^{-S}, \tag{103}$$

where

$$\begin{aligned}
S &= S_{0,a} + S_{0,b} + S_2 + S_4 \\
&= \int_0^{\infty} d\tau (\mathcal{L}_{0,a} + \mathcal{L}_{0,b} + \mathcal{L}_2 + \mathcal{L}_4), \tag{104}
\end{aligned}$$

$$\mathcal{L}_{0,a} = \sum_{\mathbf{R},\sigma} \left[a_{\sigma}^{\dagger}(\mathbf{R}, \tau) \left(\frac{\partial}{\partial \tau} + H_a - \mu \right) a_{\sigma}(\mathbf{R}, \tau) \right], \tag{105}$$

$$\mathcal{L}_{0,b} = \sum_{\mathbf{R},\sigma} \left[b_{\sigma}^{\dagger}(\mathbf{R}, \tau) \left(\frac{\partial}{\partial \tau} - \mu \right) b_{\sigma}(\mathbf{R}, \tau) \right], \tag{106}$$

$$\mathcal{L}_2 = -t \sum_{\mathbf{R},\delta,\sigma} [b_{1\sigma}^*(\mathbf{R} + \delta, \tau) a_{1\sigma}(\mathbf{R}, \tau) + b_{2\sigma}^*(\mathbf{R} - \delta, \tau) a_{2\sigma}(\mathbf{R}, \tau) + \text{c.c.}], \tag{107}$$

$$\begin{aligned}
\mathcal{L}_4 &= \frac{1}{2} \sum_{k=1}^2 \sum_{\mathbf{R} \neq \mathbf{R}'} V(\mathbf{R} - \mathbf{R}' - (-1)^{k-1} \delta) [n_{ak}(\mathbf{R}, \tau) n_{bk}(\mathbf{R}' + (-1)^{k-1} \delta, \tau) - n_{ak}(\mathbf{R}, \tau) - n_{bk}(\mathbf{R}' + (-1)^{k-1} \delta, \tau)] \\
&+ \frac{1}{2} \sum_{k=1}^2 \sum_{\mathbf{R} \neq \mathbf{R}'} V(\mathbf{R} - \mathbf{R}') [n_{ak}(\mathbf{R}, \tau) n_{ak}(\mathbf{R}', \tau) - 2n_{ak}(\mathbf{R}, \tau)] \\
&+ V(0) \sum_{k=1}^2 \sum_{\mathbf{R}} [n_{ak\uparrow}(\mathbf{R}, \tau) n_{ak\downarrow}(\mathbf{R}', \tau) - \frac{1}{2} n_{ak}(\mathbf{R}, \tau)] \\
&+ \frac{1}{2} \sum_{k=1}^2 \sum_{\mathbf{R} \neq \mathbf{R}'} V(\mathbf{R} - \mathbf{R}') [n_{bk}(\mathbf{R} + (-1)^{k-1} \delta, \tau) n_{bk}(\mathbf{R}' + (-1)^{k-1} \delta, \tau) - 2n_{bk}(\mathbf{R} + (-1)^{k-1} \delta, \tau)] \\
&+ V(0) \sum_{k=1}^2 \sum_{\mathbf{R}} [n_{bk\uparrow}(\mathbf{R} + (-1)^{k-1} \delta, \tau) n_{bk\downarrow}(\mathbf{R}' + (-1)^{k-1} \delta, \tau) - \frac{1}{2} n_{bk}(\mathbf{R} + (-1)^{k-1} \delta, \tau)] \\
&+ \sum_{\mathbf{R}\mathbf{R}'} V_{\perp}(\mathbf{R} - \mathbf{R}') [n_{a1}(\mathbf{R}, \tau) n_{a2}(\mathbf{R}', \tau) - n_{a1}(\mathbf{R}, \tau) - n_{a2}(\mathbf{R}', \tau)] \\
&+ \sum_{\mathbf{R}\mathbf{R}'} V_{\perp}(\mathbf{R} - \mathbf{R}' + \delta) [n_{b1}(\mathbf{R} + \delta, \tau) n_{a2}(\mathbf{R}', \tau) - n_{b1}(\mathbf{R} + \delta, \tau) - n_{a2}(\mathbf{R}', \tau)] \\
&+ \sum_{\mathbf{R}\mathbf{R}'} V_{\perp}(\mathbf{R} - \mathbf{R}' + \delta) [n_{a1}(\mathbf{R}, \tau) n_{b2}(\mathbf{R}' - \delta, \tau) - n_{a1}(\mathbf{R}, \tau) - n_{b2}(\mathbf{R}' - \delta, \tau)] \\
&+ \sum_{\mathbf{R}\mathbf{R}'} V_{\perp}(\mathbf{R} - \mathbf{R}' + 2\delta) [n_{b1}(\mathbf{R} + \delta, \tau) n_{b2}(\mathbf{R}' - \delta, \tau) - n_{b1}(\mathbf{R} + \delta, \tau) - n_{b2}(\mathbf{R}' - \delta, \tau)], \tag{108}
\end{aligned}$$

and H_a is the same matrix as in the spinless case. Here, we define

$$a_{\sigma}(\mathbf{R}, \tau) = \begin{bmatrix} a_{1\sigma}(\mathbf{R}, \tau) \\ a_{2\sigma}(\mathbf{R}, \tau) \end{bmatrix} \tag{109}$$

and similarly for $b_{\sigma}(\mathbf{R}, \tau)$. We also define $n_{ak}(\mathbf{R}, \tau) = \sum_{\sigma} a_{k\sigma}^*(\mathbf{R}, \tau) a_{k\sigma}(\mathbf{R}, \tau)$, and similarly for $n_{bk}(\mathbf{R}, \tau)$.

From this point forward, we will set μ to zero so that our system is at half filling, as stated above.

We may now perform the cumulant expansion, as we did with the spinless case. The details are very similar to what is presented above, except that we only go to

first order in the interaction for reasons stated earlier; we must still go to second order in the cumulant expansion to generate the “kinetic” term. Performing this expansion, we find that our effective Lagrangian is

$$\begin{aligned}
\mathcal{L}_{\text{eff}} &= \sum_{\mathbf{R}, \sigma} \left[b_{\sigma}^{\dagger}(\mathbf{R}, \tau) \frac{\partial}{\partial \tau} b_{\sigma}(\mathbf{R}, \tau) \right] + \frac{t^2}{t_{\perp}} \sum_{\mathbf{R}, \delta, \delta', \sigma} [b_1^*(\mathbf{R} + \delta, \tau) b_2(\mathbf{R} - \delta', \tau) + b_2^*(\mathbf{R} - \delta, \tau) b_1(\mathbf{R} + \delta', \tau)] \\
&+ \frac{1}{2} \sum_{k=1}^2 \sum_{\mathbf{R} \neq \mathbf{R}'} V(\mathbf{R} - \mathbf{R}') [n_{bk}(\mathbf{R} + (-1)^{k-1} \delta, \tau) n_{bk}(\mathbf{R}' + (-1)^{k-1} \delta, \tau) - 2n_{bk}(\mathbf{R} + (-1)^{k-1} \delta, \tau)] \\
&+ V(0) \sum_{k=1}^2 \sum_{\mathbf{R}} [n_{bk\uparrow}(\mathbf{R} + (-1)^{k-1} \delta, \tau) n_{bk\downarrow}(\mathbf{R}' + (-1)^{k-1} \delta, \tau) - \frac{1}{2} n_{bk}(\mathbf{R} + (-1)^{k-1} \delta, \tau)] \\
&+ \sum_{\mathbf{R}\mathbf{R}'} V_{\perp}(\mathbf{R} - \mathbf{R}' + 2\delta) [n_{b1}(\mathbf{R} + \delta, \tau) n_{b2}(\mathbf{R}' - \delta, \tau) - n_{b1}(\mathbf{R} + \delta, \tau) - n_{b2}(\mathbf{R}' - \delta, \tau)]. \tag{110}
\end{aligned}$$

We will now write a theory for modes near the parabolic degeneracy points. To do this, we first perform a Fourier transform of the fields with respect to position:

$$b_{i\sigma}(\mathbf{R}, \tau) = \frac{1}{\sqrt{N}} \sum_{\mathbf{k}} b_{i\sigma}(\mathbf{k}, \tau), \tag{111}$$

where N is the number of unit cells in our system. Performing the same procedure as before, we find that the non-interacting part of our effective Lagrangian \mathcal{L}_0 becomes

$$\mathcal{L}_0 = \frac{1}{A_{uc}} \int d^2 \mathbf{r} \left[\psi^{\dagger}(\mathbf{r}, \tau) \left(\frac{\partial}{\partial \tau} + \sum_{a=x,y} \Sigma^a d^a(\mathbf{p}) \right) \psi(\mathbf{r}, \tau) \right], \tag{112}$$

where A_{uc} is the area of a unit cell. In this case, however, the field ψ is now an eight-component field, given by

$$\psi(\mathbf{r}, \tau) = \frac{1}{\sqrt{N}} \sum_{\mathbf{q}} \psi(\mathbf{q}, \tau) e^{i\mathbf{q} \cdot \mathbf{r}}, \tag{113}$$

where

$$\psi(\mathbf{q}, \tau) = \begin{bmatrix} \psi_{\uparrow}(\mathbf{q}, \tau) \\ \psi_{\downarrow}(\mathbf{q}, \tau) \end{bmatrix} \tag{114}$$

and

$$\psi_{\sigma}(\mathbf{q}, \tau) = \begin{bmatrix} b_{1\sigma}(\mathbf{K} + \mathbf{q}, \tau) \\ b_{2\sigma}(\mathbf{K} + \mathbf{q}, \tau) \\ b_{1\sigma}(-\mathbf{K} + \mathbf{q}, \tau) \\ b_{2\sigma}(-\mathbf{K} + \mathbf{q}, \tau) \end{bmatrix}, \tag{115}$$

and the matrices Σ^x and Σ^y are now $\Sigma^x = 1_2 \sigma^x 1_2 = \gamma_2 \otimes 1_2$ and $\Sigma^y = \tau^z \sigma^y 1_2 = \gamma_1 \otimes 1_2$. In these definitions, the first two matrices, the τ and σ matrices, act in the valley and layer subspaces, as before, while the third matrix, which is the identity for both, acts in the spin subspace. The quantities $d^x(\mathbf{p})$ and $d^y(\mathbf{p})$ are the same as before. This theory will serve as the Gaussian fixed point for our RG calculations.

We will now consider the interaction terms. We follow a similar procedure as in the spinless case, and eventually arrive at the following effective Lagrangian:

$$\begin{aligned}
\mathcal{L}_{\text{eff}} &= \frac{1}{A_{uc}} \int d^2 \mathbf{R} \psi^{\dagger} \left[\frac{\partial}{\partial \tau} + H(\mathbf{p}) \right] \psi \\
&+ \frac{1}{2A_{uc}} \int d^2 \mathbf{R} \sum_{k=1}^2 \{ V_0 (\psi^{\dagger} \mathcal{M}_k^{(f)} \psi)^2 + V_K [(\psi^{\dagger} [\mathcal{M}_k^{(b)}]^T \psi) (\psi^{\dagger} \mathcal{M}_k^{(b)} \psi) + (\psi^{\dagger} \mathcal{M}_k^{(b)} \psi) (\psi^{\dagger} [\mathcal{M}_k^{(b)}]^T \psi)] \} \\
&+ \frac{V_{\perp, N}}{A_{uc}} \int d^2 \mathbf{R} (\psi^{\dagger} \mathcal{M}_1^{(f)} \psi) (\psi^{\dagger} \mathcal{M}_2^{(f)} \psi) - \mu' \int d^2 \mathbf{R} \psi^{\dagger} \psi, \tag{116}
\end{aligned}$$

where $\mathcal{M}_k^{(f)} = M_k^{(f)} \otimes 1_2$, $\mathcal{M}_k^{(b)} = M_k^{(f)} \otimes 1_2$, $M_k^{(f)}$ and $M_k^{(b)}$ are defined by Equations (60) and (61), and V_0 , V_K , and $V_{\perp,N}$ are defined in Equations (68)–(71). The same considerations that applied to the spinless case regarding “mixed” terms and the quadratic, chemical potential-like term apply here as well.

C. RG analysis of the theory

We will now perform our RG analysis of the theory. As was shown by one of us⁶, there are nine independent coupling constants in our theory due to the symmetries of the underlying lattice and Fierz identities. Again following the previous work⁶, we choose the following form for the interaction:

$$\frac{1}{2} \sum_{S \in \mathcal{G}} g_S \int d^2\mathbf{R} (\psi^\dagger S \psi)^2, \quad (117)$$

where $\mathcal{G} = \{A_1 \otimes 1_2, A_2 \otimes 1_2, D_1 \otimes 1_2, B_1 \otimes 1_2, C_2 \otimes 1_2, B_2 \otimes 1_2, C_1 \otimes 1_2, D_2 \otimes 1_2, A_3 \otimes 1_2, B_3 \otimes 1_2, A_4 \otimes 1_2, B_4 \otimes 1_2, C_4 \otimes 1_2, D_4 \otimes 1_2, C_3 \otimes 1_2, D_3 \otimes 1_2\}$, and the corresponding coupling constants g_S are, in order of appearance, and using the notation of the previous work⁶,

$$\{g_{A_1}^{(c)}, g_{A_2}^{(c)}, g_{A_2}^{(c)}, g_{B_1}^{(c)}, g_{B_1}^{(c)}, g_{B_2}^{(c)}, g_{C_1}^{(c)}, g_{D_2}^{(c)}, g_{\alpha}^{(c)}, g_{\alpha}^{(c)}, g_{\beta}^{(c)}, g_{\beta}^{(c)}, g_{\beta}^{(c)}, g_{\beta}^{(c)}, g_{\gamma}^{(c)}, g_{\gamma}^{(c)}\}. \quad (118)$$

When we rewrite our theory in the this form, we find that

$$g_{A_1}^{(c)} = \frac{V_0 + V_{\perp,N}}{2A_{uc}}, \quad (119)$$

$$g_{C_1}^{(c)} = \frac{V_0 - V_{\perp,N}}{2A_{uc}}, \quad (120)$$

$$g_{\beta}^{(c)} = \frac{V_K}{4A_{uc}}, \quad (121)$$

and all of the other coupling constants are zero. We note that $g_{A_1}^{(c)}$ and $g_{C_1}^{(c)}$ depend only on $\mathbf{q} = 0$ Fourier components of the interaction, and thus we may say that they give us a measure of the strength of the forward scattering induced by said interaction. Likewise, we note that $g_{\beta}^{(c)}$ only depends on the $\mathbf{q} = \pm 2\mathbf{K}$ Fourier components, and thus we may say that it gives us a measure of the strength of the back scattering. Furthermore, we see that $g_{C_1}^{(c)}$ depends on the difference between an intra-layer interaction and an inter-layer interaction, and thus it may be seen as a measure of the imbalance between these two interactions.

We consider the same two interactions as before, given by Equations (81) and (82). The flows of these constants is determined by the equations derived by one of us; they are found in Appendix A of Ref.⁶.

We determine the phase that our system enters for a given range of the interaction through a similar method as before. However, in this case, we allow the coupling constants to run until one constant reaches a certain fixed

value. To be exact, we stop the flow when one constant satisfies

$$\frac{mA_{uc}}{4\pi} |g| = g_{\text{cutoff}}, \quad (122)$$

where $g_{\text{cutoff}} < 1$. At this point, we find the susceptibilities toward different orders as before, and the order with the largest susceptibility is the one that is assumed to be present. In the previous work, only particle-hole channels were considered in the spin- $\frac{1}{2}$ case⁶; we will also consider particle-particle channels here. For these channels, we require that the integral,

$$\int d^2\mathbf{R} \psi_a(\mathbf{R}, \tau) \mathcal{O}_{i,ab} \psi_b(\mathbf{R}, \tau), \quad (123)$$

be non-zero. In order for this to be possible, the matrix \mathcal{O}_i must be antisymmetric. As pointed out in the previous work⁶, in the spinless case, there are six SU(4) generators that satisfy this condition; the other ten are symmetric. In the spin- $\frac{1}{2}$ case, however, our matrices \mathcal{O}_i are of the form $O_i \otimes 1_2$ and $O_i \otimes \sigma^a$, where O_i is an SU(4) generator and $a = (x, y, z)$. Matrices of the form $O_i \otimes 1_2$, $O_i \otimes \sigma^x$, or $O_i \otimes \sigma^z$ will possess the same symmetry as O_i , while those of the form $O_i \otimes \sigma^y$ will possess the opposite symmetry. In the former case, our choice of O_i must be one of the six antisymmetric SU(4) generators; we identify the corresponding orders as triplet superconducting orders. In the latter case, we must instead choose O_i to be one of the ten symmetric SU(4) generators; the corresponding orders are singlet superconducting orders. In all, we have $3 \times 6 + 10 = 28$ different order parameters to consider.

We find the susceptibilities by a similar procedure as before; we once again obtain Equation (91), only now the sum over M is over nine different couplings, namely A_1 , A_2 , B_1 , B_2 , C_1 , D_2 , α , β , and γ . The coefficients C_M that occur in this equation are listed in Table I.

D. Determination of Phases

We are now ready to find the phases that our system enters. We use the same parameters as before. Since we are using a fixed cutoff value for the RG flows of our coupling constants, we will find that the range at which a given phase transition happens will depend on the value of the cutoff; we therefore plot the phases as a function of both the interaction range and the cutoff; the generic phase diagram obtained was shown in Figure 2.

1. Screened Coulomb-like interaction; two-plate case

In the case of the screened Coulomb-like interaction, the on-site interaction given by our formula is infinite. We recognize that, for two electrons on the lattice that are sufficiently close, the electrons are not localized at a

(Singlet)	1	2	3	4
Δ_A	-1, 0, 0, -1, -1, -1, 0, 0, 0	-2, -4, -4, -2, 2, 2, 0, 0, 0	-1, 0, 0, 1, 1, -1, -2, 0, -2	-2, -4, 4, 2, -2, 2, -4, -8, 4
Δ_B	-2, -4, -4, -2, 2, 2, 0, 0, 0	-1, 0, 0, -1, -1, -1, 0, 0, 0	—	—
Δ_C	-1, 0, 0, -1, -1, -1, 0, 0, 0	—	—	0, 0, 0, 0, 0, 0, 0, 0, 0
Δ_D	—	-1, 0, 0, -1, -1, -1, 0, 0, 0	-1, 0, 0, 1, 1, -1, -2, 0, -2	—
(Triplet)	1	2	3	4
Δ_A	—	—	—	—
Δ_B	—	—	-1, 0, 0, 1, 1, -1, 2, 0, 2	-2, -4, 4, 2, -2, 2, 4, 8, -4
Δ_C	—	0, 0, 0, 0, 0, 0, 0, 0, 0	-1, 0, 0, 1, 1, -1, 2, 0, 2	—
Δ_D	0, 0, 0, 0, 0, 0, 0, 0, 0	—	—	0, 0, 0, 0, 0, 0, 0, 0, 0

TABLE I: Coefficients C_M occurring in Equation (91) for the susceptibilities to different particle-particle orders. These coefficients are, in order of appearance, for g_{A_1} , g_{A_2} , g_{B_1} , g_{B_2} , g_{C_1} , g_{D_2} , g_α , g_β , and g_γ .

single point, but rather their wave functions have a finite extent in space. This will render the on-site interaction finite. As a simple model of this effect, we set the on-site interaction equal to some constant λ times the nearest-neighbor interaction. In our calculations, we set $\lambda = 1.2$.

Using the parameters stated above, we find that the system will enter an antiferromagnetic phase for shorter ranges and a nematic phase for longer ranges, in agreement with the previous work^{5,6}, for both forms of the interaction.

Under certain conditions, however, we find that, in addition to the antiferromagnetic and nematic phases mentioned above, the system may also enter a quantum spin Hall phase for certain intermediate ranges. Let us suppose that we set λ to a value less than 1; that is, we make the on-site interaction *weaker* than the nearest-neighbor interaction. We will find that, for certain values of the interaction range, the initial value of the coupling g_β becomes negative. In such cases, we find that the system enters the quantum spin Hall phase.

2. Screened Coulomb-like interaction; one-plate case (dipole-like interaction)

For the spin- $\frac{1}{2}$ case, we consider, in addition to the interaction considered above and the exponential interaction that we will discuss below, a dipole-like interaction much like the one produced by an electron in the presence of a single infinite conducting plate. This interaction has the form,

$$V(\mathbf{r}) = U_0 \left[\frac{1}{r/\xi} - \frac{1}{\sqrt{(r/\xi)^2 + 1}} \right], \quad (124)$$

This interaction has a longer range than the previous interaction, since this falls off as r^{-3} for long distances, rather than as an exponential. As in the previous case, this formula, as is, will give us an infinite on-site interaction. We use the same model as before to render this interaction finite, and we again set $\lambda = 1.2$. In this case, we obtain the same phases as before, but now the value of

ξ at which we see the transition for a given initial value of g_{A_1} is roughly half what we would obtain in the previous case; this is illustrated in Figure 4.

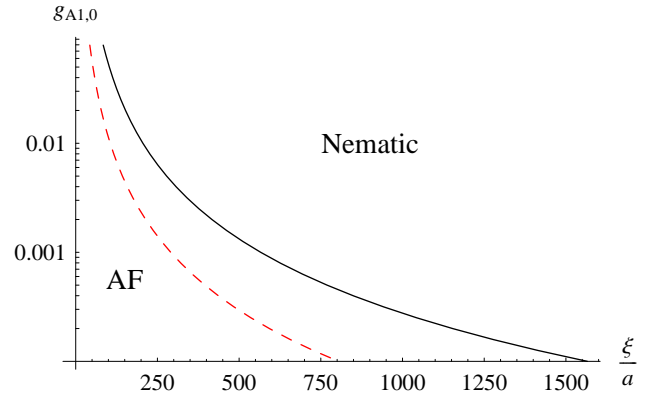


FIG. 4: Comparison of the boundary between the antiferromagnetic (AF) phase and the nematic phase for the screened Coulomb-like interaction (solid line) and that for the dipole-like interaction (dashed line). We see that the transition from the antiferromagnetic phase to the nematic phase for a given initial value of the coupling g_{A_1} for the dipole-like interaction occurs at a value of ξ that is roughly half that for the screened Coulomb-like interaction.

3. Exponential interaction

Unlike the previous two cases, there is no divergence of the on-site interaction in the exponential case. Again using the parameters stated above, we find that the phase diagram for this interaction is qualitatively the same as that for the previous two cases; however, the ranges at which the phase transition from the antiferromagnetic phase to the nematic phase are different.

4. Quantum anomalous Hall phase?

We also consider the problem of finding under what conditions we may obtain a quantum anomalous Hall phase (that is, a finite expectation value of $D_2 \otimes 1_2$). It was shown by one of us and Yang⁵ that one fixed point for the RG flows in the spin- $\frac{1}{2}$ case corresponds to this phase, and it turns out that this fixed point is completely stable. At this fixed point, the coupling constant ratio $\frac{g_{D_2}}{g_{A_2}} \approx 13.98$, with all other ratios tending to zero⁵. For this reason, we searched for an interaction in terms of the low-energy modes b that would produce a term of the form,

$$g_{D_2} \int d^2\mathbf{R} (\psi^\dagger (D_2 \otimes 1_2) \psi)^2, \quad (125)$$

in the effective low-energy theory. One such interaction is

$$V_b \sum_{\mathbf{r}} B^*(\mathbf{r}) B(\mathbf{r}), \quad (126)$$

where

$$B(\mathbf{r}) = \sum_{\epsilon} \sin(\mathbf{K} \cdot \epsilon) [b_{1\sigma}^*(\mathbf{r} + \epsilon) b_{1\sigma}(\mathbf{r} + \delta) - b_{2\sigma}^*(\mathbf{r} - \delta + \epsilon) b_{2\sigma}(\mathbf{r} - \delta)] \quad (127)$$

and ϵ runs over all vectors pointing to nearest neighbors to a site on a triangular lattice. If we apply the same procedure as before to this interaction as we did to derive the effective low-energy theory, we find that this gives us the above form, with

$$g_{D_2} = -\frac{9V_b}{4A_{uc}}. \quad (128)$$

Currently, we can only speculate about what sort of interaction would produce a term of this form in our theory. We found the phases that the system will enter if this interaction is introduced for both forms of the finite-range interaction, as before; the phase diagram for the screened Coulomb-like interaction is shown in Figure 5.

IV. ANALYSIS OF THE ANTIFERROMAGNETIC STATE IN AN APPLIED MAGNETIC FIELD

We now turn our attention to the effects of a magnetic field on the antiferromagnetic state of the spin- $\frac{1}{2}$ system at zero temperature. We will investigate these effects within the framework of variational mean field theory. We start by writing down a Hamiltonian corresponding to our effective low-energy field theory and introducing the orbital effects of the magnetic field via minimal substitution. We will neglect the Zeeman effect in this case, since we expect it to be small compared to the orbital

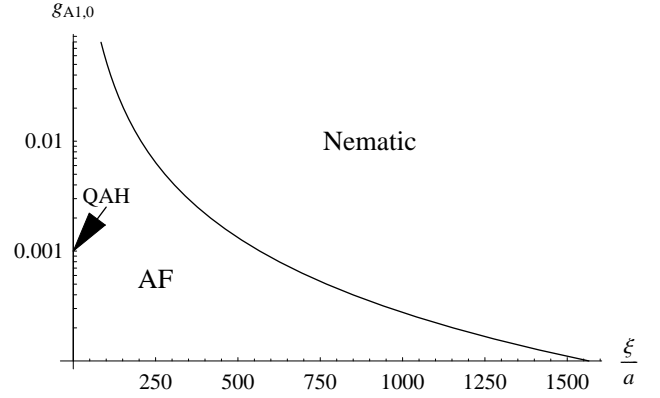


FIG. 5: Phase diagram for spin- $\frac{1}{2}$ fermions on a honeycomb bilayer with a screened Coulomb-like interaction and the “bond interaction” given by Equation (126). We see that, for very short ranges of the interaction, we enter a quantum anomalous Hall (QAH) phase before going into the antiferromagnetic phase. The quantum anomalous Hall phase occurs for ranges $\xi \leq 0.122a$. For the exponential interaction, the quantum anomalous Hall phase occurs for a much larger value of ξ , of order $10a$, while the antiferromagnetic-to-nematic transition occurs at much smaller values of ξ .

effects. This Hamiltonian is

$$H = \int d^2\mathbf{r} \psi^\dagger(\mathbf{r}) \left(\sum_{a=x,y} d^a(\boldsymbol{\pi}) \Sigma^a \right) \psi(\mathbf{r}) + \frac{1}{2} \sum_{S,T} \int d^2\mathbf{r} g'_{ST} [\psi^\dagger(\mathbf{r}) S \psi(\mathbf{r})] [\psi^\dagger(\mathbf{r}) T \psi(\mathbf{r})] \quad (129)$$

where $\boldsymbol{\pi} = \mathbf{p} - \frac{e}{c} \mathbf{A}$, \mathbf{A} is the applied magnetic vector potential,

$$d^x(\boldsymbol{\pi}) = \frac{\pi_x^2 - \pi_y^2}{2m}, \quad d^y(\boldsymbol{\pi}) = \frac{\pi_x \pi_y + \pi_y \pi_x}{2m}, \quad (130)$$

and the sum on S and T stands for the four-fermion interaction terms that appear in Equation (116). Here, ψ is a field operator, not a Grassman field as it was in previous sections. Also note that we have rescaled the fields relative to previous sections; we absorbed a factor of $\frac{1}{\sqrt{A_{uc}}}$ into each field.

Our variational mean field calculation will proceed as follows. We start by adding and subtracting a source term for the antiferromagnetic order parameter,

$$\Delta \int d^2\mathbf{r} \psi^\dagger(\mathbf{r}) (C_1 \otimes \sigma^z) \psi(\mathbf{r}), \quad (131)$$

in the Hamiltonian. We now define two parts to the Hamiltonian, a “non-interacting” part, H_0 ,

$$H_0 = \int d^2\mathbf{r} \psi^\dagger(\mathbf{r}) \left(\sum_{a=x,y} d^a(\boldsymbol{\pi}) \Sigma^a \right) \psi(\mathbf{r}) + \Delta \int d^2\mathbf{r} \psi^\dagger(\mathbf{r}) (C_1 \otimes \sigma^z) \psi(\mathbf{r}), \quad (132)$$

and an “interaction”, H_I ,

$$H_I = \frac{1}{2} \sum_{S,T} \int d^2\mathbf{r} g'_{ST} [\psi^\dagger(\mathbf{r}) S \psi(\mathbf{r})] [\psi^\dagger(\mathbf{r}) T \psi(\mathbf{r})] - \Delta \int d^2\mathbf{r} \psi^\dagger(\mathbf{r}) (C_1 \otimes \sigma^z) \psi(\mathbf{r}). \quad (133)$$

We then exactly diagonalize H_0 , find the expectation value of the full Hamiltonian with respect to the ground state of H_0 , and minimize the result with respect to Δ . We will provide the details of the diagonalization in an appendix, and simply quote the main result here. We find that our states can be described in terms of a wave number k , an orbital index n , a valley index τ , and a spin index s ; the corresponding energy eigenvalues are $E_n = \pm \sqrt{n(n-1)\omega_c^2 + \Delta^2}$, where $\omega_c = \frac{eB}{mc}$ is the cyclotron frequency of the electrons. For $n \geq 2$, each of these energy levels is four-fold degenerate due to valley and spin degeneracies. The levels given by $n = 0$ and 1 are also four-fold degenerate, but this time due to *orbital* ($n = 0$ or 1) and spin degeneracies.

We may now rewrite the field operators in terms of these eigenstates:

$$\psi(x, y) = \sum_{k,n,\tau,s} [\psi_{k,n,\tau,s}^+(x, y) a_{k,n,\tau,s} + \psi_{k,n,\tau,s}^-(x, y) b_{k,n,\tau,s}^\dagger], \quad (134)$$

where $\psi_{k,n,\tau,s}^{+(-)}$ represents the positive (negative) energy state for a given wave number and orbital, valley, and spin indices. We have chosen our operators a and b such that they annihilate the ground state $|0\rangle$. We may now take the expectation value of our Hamiltonian with respect to the ground state of H_0 and minimize the result with respect to Δ ; we provide details on the procedure in Appendix C. Upon doing so, we find that the equation for Δ is

$$g_{\text{eff}} \omega_c \left(\sum_{n=2}^N \frac{\Delta}{E_n} + \text{sgn } \Delta \right) = \Delta, \quad (135)$$

where

$$g_{\text{eff}} = \frac{m}{4\pi} (V_0 + V_{2K}) \quad (136)$$

and N is an upper cutoff on the orbital index, which we impose because our theory only works for low energies and because, in reality, we do not have electronic states in our system at arbitrarily large energies. In the limit of zero magnetic field, we may treat the sum as a Riemann sum, with $\epsilon = n\omega_c$ and $\Delta\epsilon = \omega_c$; our equation then reduces to

$$g_{\text{eff}} \omega_c \int_0^\Omega \frac{d\epsilon}{\sqrt{\epsilon^2 + \Delta^2}} = 1, \quad (137)$$

where Ω is an upper cutoff on the energy; N is related to this cutoff by $\Omega = \omega_c \sqrt{N(N-1)}$. We have verified this result with a separate calculation. As is, we cannot

send our upper cutoff to infinity without encountering a divergence in our sum, since the summand only decreases as $\frac{1}{n}$. We can, however, rewrite the equation in such a way that we can do this. We start by rewriting the sum as an integral over a “Dirac comb”:

$$\omega_c \left(\int_{3/2}^N d\lambda \frac{1}{\sqrt{\lambda(\lambda-1)\omega_c^2 + \Delta^2}} \sum_{n=-\infty}^{\infty} \delta(\lambda - n) + \frac{1}{|\Delta|} \right) = \frac{1}{g_{\text{eff}}}. \quad (138)$$

We now use the identity,

$$\sum_{n=-\infty}^{\infty} \delta(\lambda - n) = \sum_{k=-\infty}^{\infty} e^{2\pi i k \lambda}, \quad (139)$$

to obtain

$$\begin{aligned} & \omega_c \int_{3/2}^N d\lambda \frac{1}{\sqrt{\lambda(\lambda-1)\omega_c^2 + \Delta^2}} + \\ & + 2\omega_c \sum_{k=1}^{\infty} \int_{3/2}^N d\lambda \frac{\cos(2\pi k \lambda)}{\sqrt{\lambda(\lambda-1)\omega_c^2 + \Delta^2}} + \frac{\omega_c}{|\Delta|} \\ & = \frac{1}{g_{\text{eff}}}. \end{aligned} \quad (140)$$

The integral that appears in the sum converges for all $k \geq 1$, so we may already send the upper limit to infinity. However, we must still take care of the first integral, which will diverge if we do the same with it. We may use the zero-field equation, Equation (137), to rewrite the right-hand side such that we eliminate g_{eff} from the equation. If we do this and also introduce the change of variables, $\epsilon^2 = \lambda(\lambda-1)\omega_c^2$, into the first integral, we may then move the first integral to the right-hand side, obtaining an integral that converges if we send the upper limit to infinity, namely

$$\begin{aligned} & \omega_c \int_0^\infty d\lambda \left(\frac{1}{\sqrt{\epsilon^2 + \Delta_0^2}} - \frac{\epsilon}{\sqrt{\epsilon^2 + \frac{1}{4}\omega_c^2}} \frac{1}{\sqrt{\epsilon^2 + \Delta^2}} \right) + \\ & + \omega_c \int_0^{\omega_c \sqrt{3/2}} d\lambda \frac{\epsilon}{\sqrt{\epsilon^2 + \frac{1}{4}\omega_c^2}} \frac{1}{\sqrt{\epsilon^2 + \Delta^2}}, \end{aligned} \quad (141)$$

where Δ_0 is the value of Δ at zero magnetic field. Upon evaluating this integral, our equation becomes

$$\begin{aligned} & 2\omega_c \sum_{k=1}^{\infty} \int_{3/2}^{\infty} d\lambda \frac{\cos(2\pi k \lambda)}{\sqrt{\lambda(\lambda-1)\omega_c^2 + \Delta^2}} + \frac{\omega_c}{|\Delta|} \\ & = \ln \left(\frac{\omega_c}{\Delta_0} + \frac{\sqrt{\Delta^2 + \frac{3}{4}\omega_c^2}}{\Delta_0} \right). \end{aligned} \quad (142)$$

This equation may be rewritten in terms of the dimensionless parameters, $\alpha = \Delta/\omega_c$ and $\beta = \omega_c/\Delta_0$:

$$2 \sum_{k=1}^{\infty} \int_{3/2}^{\infty} d\lambda \frac{\cos(2\pi k \lambda)}{\sqrt{\lambda(\lambda-1) + \alpha^2}} + \frac{1}{|\alpha|} - \ln \left(1 + \sqrt{\alpha^2 + \frac{3}{4}} \right)$$

= $\ln \beta$.

(143) where

We can see that the left-hand side is a monotonically-decreasing function of α for $\alpha > 0$. In fact, as $\alpha \rightarrow 0^+$, the left-hand side increases indefinitely due to the second term, while, as $\alpha \rightarrow \infty$, the expression decreases indefinitely due to the third term. This equation therefore has a single positive solution for α for any given value of β . While we would need to solve the equation numerically for general values of β , we can derive approximate solutions analytically for very large and very small values of β .

Before we do this, however, let us first rewrite this equation in an equivalent form. We start by changing variables in the first term to $x = \lambda - \frac{1}{2}$, obtaining

$$2 \sum_{k=1}^{\infty} (-1)^k \operatorname{Re} \int_1^{\infty} dx \frac{e^{2\pi i k x}}{\sqrt{x^2 + \alpha^2 - \frac{1}{4}}} + \frac{1}{|\alpha|} - \ln \left(1 + \sqrt{\alpha^2 + \frac{3}{4}} \right) = \ln \beta.$$

We now note that, as a function of x , the integral is analytic in the entire complex plane, except for a branch cut. For $\alpha < \frac{1}{2}$, this branch cut can be chosen to be on the real axis and in the interval $-\sqrt{\frac{1}{4} - \alpha^2} < x < \sqrt{\frac{1}{4} - \alpha^2}$. For $\alpha > \frac{1}{2}$, on the other hand, the branch cut may be chosen to lie along the imaginary axis. In either case, we may integrate this function over a large quarter circle centered at the point, $x = 1$, in the complex plane and with one of the radii along the positive real axis and the other parallel to the positive imaginary axis and obtain zero since we will always avoid the branch cut. The contribution from the circular arc will vanish as we increase the radius to infinity since the integrand decreases exponentially as we do so. This leaves only contributions from the radii. The contribution from the radius along the real axis is just the integral that appears in the equation. This means that the contribution from the radius parallel to the imaginary axis is equal to this integral. We may therefore write

$$\begin{aligned} & \operatorname{Re} \int_1^{\infty} dx \frac{e^{2\pi i k x}}{\sqrt{x^2 + \alpha^2 - \frac{1}{4}}} \\ &= \operatorname{Re} \left[i \int_0^{\infty} dx' \frac{e^{-2\pi k x'}}{\sqrt{(1 + ix')^2 + \alpha^2 - \frac{1}{4}}} \right]. \end{aligned}$$

Note that we dropped a factor of $e^{-2\pi i k}$; since k is an integer, this factor is always equal to 1. If we substitute this back into the equation, we find that the sum on k is just a geometric series with a common ratio of $-e^{-2\pi x'}$. We may therefore perform the summation, obtaining

$$I(\alpha) + \frac{1}{|\alpha|} - \ln \left(1 + \sqrt{\alpha^2 + \frac{3}{4}} \right) = \ln \beta, \quad (144)$$

$$I(\alpha) = -2 \operatorname{Re} \left[i \int_0^{\infty} dx' \frac{1}{\sqrt{(1 + ix')^2 + \alpha^2 - \frac{1}{4}}} \frac{1}{e^{2\pi x'} + 1} \right].$$

We can see that the integral $I(\alpha)$ converges for all values of α ; the integrand is analytic everywhere on the interval of integration and decreases exponentially for large x' . At large values of α , we can show that this integral falls off as α^{-3} . We first note that the integral is dominated by small values of x' due to the Fermi occupation factor-like expression. With this in mind, we may pull out a factor of α from the square root, obtaining

$$-2 \operatorname{Re} \left[i \int_0^{\infty} dx' \frac{1}{\alpha} \left[1 + \frac{(1 + ix')^2 - \frac{1}{4}}{\alpha^2} \right]^{-1/2} \frac{1}{e^{2\pi x'} + 1} \right].$$

Since α is large, we now have a small parameter with respect to which we may perform an expansion of the square root. The constant term in this expansion gives no contribution, since the total result will be purely imaginary. The lowest-order non-zero contribution will, in fact, be given by

$$-\frac{2}{\alpha^3} \int_0^{\infty} dx' \frac{x'}{e^{2\pi x'} + 1} = -\frac{1}{24\alpha^3}.$$

We see that this term is of the order α^{-3} , as asserted earlier.

We may derive a good closed-form approximation to $I(\alpha)$ as follows. Let us first expand the square root in the integrand in powers of x' . To the lowest non-vanishing order, we obtain

$$I(\alpha) \approx -2 \int_0^{\infty} dx' \frac{x'}{\left(\frac{3}{4} + \alpha^2\right)^{3/2}} \frac{1}{e^{2\pi x'} + 1} = -\frac{1}{3(3 + 4\alpha^2)^{3/2}}.$$

We now rewrite this expression so that its value at $\alpha = 0$ matches the exact value of $I(0)$. Doing so, we obtain

$$I(\alpha) \approx -\frac{2}{\left[(-\frac{1}{2}I(0))^{-2/3} + 4 \cdot 6^{2/3}\alpha^2\right]^{3/2}}. \quad (145)$$

If we were to plot this expression alongside the exact expression for $I(\alpha)$, then we would see that it follows the exact expression very closely. In fact, if we use this expression to solve Equation (144), then the solution that we obtain is very close to the solution obtained from the exact $I(\alpha)$.

Let us first consider the large β limit. This means that the right-hand side of our equation is large and positive, and thus, as implied by our above discussion, α should be small. In this limit, we may set the first and third terms on the left to their values at $\alpha = 0$, since both are finite at this point, while the second term diverges. Our equation becomes

$$\frac{1}{\alpha} - C = \ln \beta, \quad (146)$$

where C is the value of the first and third terms at $\alpha = 0$; its value is approximately 0.67. Here, we are assuming that α is positive. Solving for α , we find that

$$\alpha = \frac{1}{\ln \beta + C},$$

or

$$\Delta = \frac{\omega_c}{\ln(\omega_c/\Delta_0) + C}. \quad (147)$$

We see that the behavior is almost linear in the magnetic field, but with a logarithmic correction.

Next, we consider the small β limit. In this case, the right-hand side of our equation becomes large and negative, and thus α should become large. We would be tempted to drop all but the third term, since the first two terms go to zero for large values of α . This would give us a result that is only accurate at constant order in β , however. This is because, if we expand this term in powers of α^{-1} , then the next-lowest order term after the logarithmic term is of order α^{-1} , and the second term in our equation is also of this order; in fact, it cancels this term exactly. We may still drop the first term, since, as stated above, the lowest-order term that it contributes is of order α^{-3} . In this case, our equation becomes

$$\frac{1}{\alpha} - \ln \left(1 + \sqrt{\alpha^2 + \frac{3}{4}} \right) = \ln \beta. \quad (148)$$

Again, we are assuming that $\alpha > 0$. If we take the exponential of both sides, we get

$$e^{-1/\alpha} \left(1 + \sqrt{\alpha^2 + \frac{3}{4}} \right) = \frac{1}{\beta}.$$

We will now expand the left-hand side in powers of α^{-1} to the order α^{-2} . Doing so, but first pulling out a factor of α from the second factor, we get

$$\alpha \left(1 - \frac{1}{8\alpha^2} \right) = \frac{1}{\beta}.$$

If we rearrange this, we finally arrive at the quadratic equation,

$$8\beta\alpha^2 - 8\alpha - \beta = 0.$$

If we solve this equation and take the positive solution, we get

$$\alpha = \frac{1 + \sqrt{1 + \frac{1}{2}\beta^2}}{2\beta} \approx \frac{1}{\beta} + \frac{\beta}{8}.$$

Rewriting this result in terms of Δ and ω_c , we get

$$\Delta = \Delta_0 + \frac{\omega_c^2}{8\Delta_0}. \quad (149)$$

We see that, for low fields, the antiferromagnetic order parameter increases quadratically with the field.

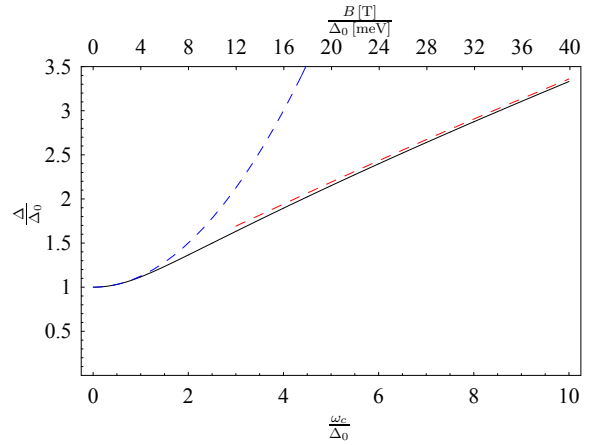


FIG. 6: Plot of the solution to Equation (143). The solid line is the numerical solution, while the dashed lines are the solutions in the low- and high-field limits. The vertical axis is the value of the order parameter Δ divided by its zero-field value Δ_0 . The bottom horizontal axis is the cyclotron frequency ω_c divided by Δ_0 , while the top horizontal axis is the applied magnetic field B divided by Δ_0 ; in determining the latter from the former, we assumed that the effective mass m of the electrons is given by the experimental value² of $0.029m_e$, where m_e is the mass of an electron.

We now solve Equation (144) numerically; the numerical result, along with the low- and high-field limits derived above, is plotted in Figure 6. If we look at our low- and high-field expressions, we see that the slope of our low-field approximation increases with B , while our high-field approximation has a decreasing slope. This implies that there should be a maximum slope to the exact curve. We determined this slope, and found that it is $1.07 \frac{\text{meV}}{\text{T}}$.

We would now like to compare our theoretical results to the experimental data⁴. First of all, we note that Δ is not the energy gap in our system, but rather 2Δ . Experimentally, the gap E_g is reported to depend on the magnetic field as

$$E_g = \Delta_0 + \sqrt{\Delta_0^2 + a^2 B^2}, \quad (150)$$

where $\Delta_0 = 1 \text{ meV}$ and $a = 5.5 \frac{\text{meV}}{\text{T}}$. At large magnetic fields, this predicts a linear increase in the gap with a slope of a , while, at low fields, it predicts a quadratic increase in the field,

$$E_g = 2\Delta_0 + \frac{a^2 B^2}{2\Delta_0}, \quad (151)$$

in qualitative agreement with our theoretical results. However, these results disagree with ours quantitatively. At low fields, we find that, assuming the experimental values of Δ_0 and of the effective electron mass² $m = 0.029m_e$, the coefficient of B^2 is $1.86 \frac{\text{meV}}{\text{T}^2}$ is about a factor of 4 smaller than the experimental result. At high field, we find that the slope of the experimental result

is about a factor of 2 larger than the maximum slope of our theoretical result. We believe that this implies that some other order emerges alongside antiferromagnetism when we apply a magnetic field, and that this other order will modify our results to be more in line with the experimental data.

There is one other point that we wish to address. Throughout this calculation, we have been assuming that the presence of the order parameter opens up a simple gap in the spectrum, modifying the low-energy dispersion to have the form, $E(\mathbf{k}) = \pm\sqrt{[\epsilon(\mathbf{k})]^2 + \Delta^2}$, where $\epsilon(\mathbf{k})$ is the dispersion in the absence of the order parameter. This assumption is, in fact, not entirely true; in reality, the dispersion acquires a ‘‘Mexican hat’’ shape. This can be seen by taking the continuum limit of the effective action in Eq.(35) which will give rise to an additional term $(v_F q/t_\perp)^2 \partial/\partial\tau$, where $v_F = \frac{3}{2}at$, in Equation (47). In the absence of an applied magnetic field, but in the presence of the antiferromagnetic order parameter Δ_0 , the dispersion is

$$E(\mathbf{k}) = \pm \frac{\sqrt{(k^2/2m)^2 + \Delta^2}}{1 + (v_F k/t_\perp)^2}. \quad (152)$$

If we expand this expression to fourth order in k , we obtain

$$E(\mathbf{k}) \approx \pm\Delta \left[1 - \left(\frac{v_F k}{t_\perp}\right)^2 + \left(\frac{v_F k}{t_\perp}\right)^4 + \frac{1}{2} \left(\frac{k^2}{2m\Delta}\right)^2 \right]. \quad (153)$$

We see that the quadratic term is negative, while the quartic term is positive, thus giving this dispersion the ‘‘Mexican hat’’ shape. Note that it is the presence of a non-zero Δ_0 that changes the scaling dimensions of our operators and necessitates the inclusion of the above-mentioned term for a complete description of the low-energy behavior. For $\Delta_0 = 0$, which is the starting point of our RG analysis, the scaling dimensions of our operators are the same as they were in Ref.⁶, which justifies neglecting this term in our RG analysis. Performing the standard minimal coupling to an external vector potential, we have looked at what effect this would have on the lowest Landau levels, and we find that it lifts the orbital degeneracy of the $n = 0$ and 1 Landau levels. To be exact, these two levels take the form,

$$E_n = \frac{\Delta}{1 + \frac{\omega_c}{t_\perp}(n + \frac{1}{2})}. \quad (154)$$

For small magnetic fields, for which $\omega_c \ll t_\perp$, we find that the splitting between these levels is approximately $\frac{\omega_c}{t_\perp}\Delta = aB$, where $a \approx 0.0106 \frac{\text{meV}}{\text{T}}$. This is small compared even to the Zeeman splitting, which is also linear in B , but with a slope of about $0.232 \frac{\text{meV}}{\text{T}}$. Therefore, we may safely neglect this effect in our calculations.

V. CONCLUSION

We have employed weak-coupling perturbative RG methods to investigate the different phases that fermions on a honeycomb bilayer lattice with finite-range interactions will enter. The use of these methods is justified since we only include nearest-neighbor hopping terms, resulting in a band structure with two quadratic degeneracy points and therefore in a finite density of states at the Fermi level at half filling. We considered three forms of the interaction, namely an exponential interaction and a screened Coulomb-like interaction much like the one produced by a point charge situated exactly halfway between two infinite parallel conducting plates, and we considered both spinless and spin- $\frac{1}{2}$ fermions. For all cases, we determined what phase the system enters as a function of the range of the interaction.

In the spinless case, we find that, for short ranges of the interaction, the system enters a layer-polarized state, in agreement with the previous work⁶. As we increase the range, the system enters a quantum anomalous Hall state, followed by a Kekulé state. In the case of a screened Coulomb-like interaction, the system returns to the layer-polarized state for long ranges of the interaction; we suspect that this should also happen for the exponential interaction, but for longer ranges than we considered.

In the spin- $\frac{1}{2}$ case, we found that the system, for an exponential interaction or for a screened Coulomb-like interaction for which the on-site interaction is made stronger than the nearest-neighbor interaction, enters an antiferromagnetic state for short ranges and a nematic state for long ranges, again in agreement with the previous work^{5,6}. In addition, we considered a dipole-like potential, much like that produced by an electron in the presence of a single conducting plate, and found that the system has a qualitatively identical phase diagram as for the screened Coulomb-like interaction, but the ranges for which the system undergoes a transition from the antiferromagnetic state to the nematic state are shorter for a given initial value of the couplings. We note that these results may help reconcile the seemingly contradictory results of two recent experiments on bilayer graphene^{2,4}. In the first experiment², only one gate was present. We argue that this modifies the electron-electron interaction, so that it now has the form of the dipole-like potential, which falls off as the inverse cube of the distance for long distances. In the second experiment⁴, on the other hand, there are two gates present; this, as we state earlier, will result in a potential that falls off exponentially with distance. This is a much shorter-ranged potential than that present in the first experiment. Our predictions are consistent with the results of these two experiments — the first reports a nematic phase, while the second reports a gapped phase, which the antiferromagnetic phase is. Interestingly, if we make the on-site interaction *weaker* than the nearest-neighbor interaction in the screened Coulomb-like case, then we may also find

a quantum spin Hall phase for intermediate ranges. We also sought out a form of an additional interaction that would cause the system to enter a quantum anomalous Hall phase, motivated by the presence of a completely stable fixed point in the RG flows that corresponds to this phase⁵.

One potential issue with the results presented is the fact that we rescaled the coupling constants before we determined the RG flows. While it appears that we may do so without qualitatively changing the resulting flows, due to the scaling property mentioned above that our RG equations possess, we must keep in mind that the original coupling constants may actually be large, which is problematic because we only determined the beta functions to second order in these constants. There is no guarantee that this scaling property will continue to hold for the exact beta functions. This fact limits us to small values of the couplings, which is part of the reason why we chose not to determine the flows in the spin- $\frac{1}{2}$ case beyond the point at which one of the couplings exceeds a certain value. We have essentially been operating under the assumption that the phase that appears to “win” at this point will continue to “win” if we were to somehow determine the exact beta functions and obtain exact RG flows that we may extend as far as we wish. It turns out that the largest coupling constant in our system, as determined from the original microscopic interaction, increases as we increase the range of the interaction. This means that we can only work with interactions up to a certain range before our (approximate) RG equations can no longer be applied.

Acknowledgments

The authors would like to acknowledge useful discussions with K. Novoselov, C. N. Lau, D. Smirnov, B. Roy, K. Yang, S. Kivelson, and S. Raghu. This work was supported in part by the NSF CAREER Award under Grant no. DMR-0955561.

Appendix A: Long-distance behavior of the screened Coulomb-like interaction

We will now demonstrate that Equation (83) is the correct long-range behavior of the screened Coulomb-like interaction, Equation (82). We start by rewriting the sum using the identity,

$$\frac{1}{r} = \frac{2}{\sqrt{\pi}} \int_0^\infty du e^{-r^2 u^2}, \quad (\text{A1})$$

obtaining

$$V(\mathbf{R}) = \frac{2}{\sqrt{\pi}} U_0 \int_0^\infty du e^{-u^2 (R/\xi)^2} \sum_{n=-\infty}^\infty (-1)^n e^{-n^2 u^2}. \quad (\text{A2})$$

We may evaluate the sum in terms of the Jacobi theta function,

$$\vartheta_4(z, q) = \sum_{n=-\infty}^\infty (-1)^n q^{n^2} e^{2niz}, \quad (\text{A3})$$

to obtain

$$V(\mathbf{R}) = \frac{2}{\sqrt{\pi}} U_0 \int_0^\infty du e^{-u^2 (R/\xi)^2} \vartheta_4(0, e^{-u^2}). \quad (\text{A4})$$

We now use the identity²⁴,

$$\begin{aligned} \vartheta_4(z, q) &= \frac{2\sqrt{\pi}}{\sqrt{-\log q}} e^{(4z^2 + \pi^2)/4 \log q} \sum_{k=0}^\infty e^{k(k+1)\pi^2 / \log q} \\ &\times \cosh \left[\frac{(2k+1)\pi z}{\log q} \right], \end{aligned} \quad (\text{A5})$$

so that

$$V(\mathbf{R}) = 4U_0 \sum_{k=0}^\infty \int_0^\infty du \frac{1}{u} e^{-u^2 (R/\xi)^2} e^{-(k+1/2)^2 \pi^2 / u^2}. \quad (\text{A6})$$

This integral can be evaluated in terms of modified Bessel functions of the second kind; the result is

$$V(\mathbf{R}) = 4U_0 \sum_{k=0}^\infty K_0 \left[(2k+1)\pi \frac{R}{\xi} \right]. \quad (\text{A7})$$

For large values of x , the modified Bessel function $K_n(x)$ can be approximated as

$$K_n(x) \approx \sqrt{\frac{\pi}{2x}} e^{-x}. \quad (\text{A8})$$

We see that, in the above sum, the most dominant term for $R \gg \xi$ is the $k=0$ term, since the values of successive terms decrease exponentially with increasing k . Therefore, we arrive at the form quoted in the main text, Equation (83).

Appendix B: Solution of the non-interacting Hamiltonian in a magnetic field with an AF order parameter

We now provide the details of the diagonalization of H_0 . To diagonalize H_0 , we first note that the source term is diagonal in layer, valley, and spin space, while the “kinetic” term is only diagonal in valley and spin space. This allows us to split the problem into the diagonalization of four 2×2 matrices; our wave functions will have a definite valley pseudospin and real spin orientation. Let us consider the block corresponding to the $+\mathbf{K}$ valley and spin up. We must solve

$$\begin{bmatrix} \Delta & \frac{(\pi_x - i\pi_y)^2}{2m} \\ \frac{(\pi_x + i\pi_y)^2}{2m} & -\Delta \end{bmatrix} \psi(x, y) = E\psi(x, y), \quad (\text{B1})$$

where $\psi(x, y)$ is a two-component spinor corresponding to the $+\mathbf{K}$ valley and spin up components of the full eight-component spinor; the other six components are all zero. We will work in the Landau gauge, in which $\mathbf{B} = -By\hat{\mathbf{x}}$. For this gauge, the above becomes

$$\begin{bmatrix} \Delta & \frac{1}{2m} (p_x + \frac{eB}{c}y - ip_y)^2 \\ \frac{1}{2m} (p_x + \frac{eB}{c}y + ip_y)^2 & -\Delta \end{bmatrix} \psi(x, y) = E\psi(x, y) \quad (\text{B2})$$

Let us now assume the following form for $\psi(x, y)$:

$$\psi(x, y) = \frac{1}{\sqrt{L_x}} e^{ikx} \Phi_k(y), \quad (\text{B3})$$

where $\Phi_k(y)$ is another two-component spinor. Upon substitution into our equation, we obtain

$$\begin{bmatrix} \Delta & \frac{1}{2m} (k + \frac{eB}{c}y - ip_y)^2 \\ \frac{1}{2m} (k + \frac{eB}{c}y + ip_y)^2 & -\Delta \end{bmatrix} \Phi_k(y) = E\Phi_k(y) \quad (\text{B4})$$

We may now write this in terms of the operators,

$$a_k = \sqrt{\frac{m\omega_c}{2}} \left(\frac{k}{m\omega_c} + y + i \frac{p_y}{m\omega_c} \right), \quad (\text{B5})$$

where $\omega_c = \frac{eB}{mc}$ is the cyclotron frequency of the electrons in our system. These operators may be verified to satisfy the commutation relation, $[a_k, a_k^\dagger] = 1$. In terms of these operators, the equation becomes

$$\begin{bmatrix} \Delta & \omega_c (a_k^\dagger)^2 \\ \omega_c a_k^2 & -\Delta \end{bmatrix} \Phi_k(y) = E\Phi_k(y). \quad (\text{B6})$$

Let us now define normalized functions $\phi_{k,n}(y)$ such that $a_k^\dagger a_k \phi_{k,n}(y) = n\phi_{k,n}(y)$; these will just be the usual harmonic oscillator-like wave functions that emerge in the solution of the free electron gas in a magnetic field. These functions may be shown to satisfy the relations, $a_k \phi_{k,n}(y) = \sqrt{n}\phi_{k,n-1}(y)$ and $a_k^\dagger \phi_{k,n}(y) = \sqrt{n+1}\phi_{k,n+1}(y)$. We now assume the following form for $\Phi_k(y)$:

$$\Phi_k(y) = \begin{bmatrix} \alpha_{k,n} \phi_{k,n}(y) \\ \beta_{k,n} \phi_{k,n-2}(y) \end{bmatrix} \quad (\text{B7})$$

We find that this form satisfies our equation, provided that $\alpha_{k,n}$ and $\beta_{k,n}$ satisfy

$$\begin{bmatrix} \Delta & \omega_c \sqrt{n(n-1)} \\ \omega_c \sqrt{n(n-1)} & -\Delta \end{bmatrix} \begin{bmatrix} \alpha_{k,n} \\ \beta_{k,n} \end{bmatrix} = E \begin{bmatrix} \alpha_{k,n} \\ \beta_{k,n} \end{bmatrix} \quad (\text{B8})$$

and $|\alpha_{k,n}|^2 + |\beta_{k,n}|^2 = 1$. We have thus reduced the problem to solving for the eigenvalues and eigenvectors of a 2×2 matrix. The eigenvalues are $E = \pm E_n$, where

$$E_n = \sqrt{n(n-1)\omega_c^2 + \Delta^2}, \quad (\text{B9})$$

and the corresponding eigenvectors are given by

$$\alpha_{k,n} = \pm \frac{1}{\sqrt{2}} \sqrt{1 \pm \frac{\Delta}{E_n}}, \quad \beta_{k,n} = \frac{1}{\sqrt{2}} \sqrt{1 \mp \frac{\Delta}{E_n}}. \quad (\text{B10})$$

In the $-\mathbf{K}$ valley, the positions of the creation and annihilation operators a_k^\dagger and a_k will be interchanged; in this case, we must instead assume that

$$\Phi_k(y) = \begin{bmatrix} \alpha_{k,n} \phi_{k,n-2}(y) \\ \beta_{k,n} \phi_{k,n}(y) \end{bmatrix}. \quad (\text{B11})$$

This will give us the same eigenvalue problem as before. For the spin down case, we simply reverse the sign on Δ in our equations; we obtain the same eigenvalues as before, but $\alpha_{k,n}$ and $\beta_{k,n}$ will switch values. This implies that, at least for $n \geq 2$, each of our energy levels is four-fold degenerate, due to valley and spin degeneracies. For $n = 0$ or 1 , on the other hand, there is no valley degeneracy for a given spin. In these cases, the eigenfunctions are

$$\Phi_k(y) = \begin{bmatrix} \phi_{k,n}(y) \\ 0 \end{bmatrix} \quad (\text{B12})$$

in the $+\mathbf{K}$ valley and

$$\Phi_k(y) = \begin{bmatrix} 0 \\ \phi_{k,n}(y) \end{bmatrix} \quad (\text{B13})$$

in the $-\mathbf{K}$ valley. The former corresponds to the energy eigenvalue, $E = \Delta$, while the other corresponds to $E = -\Delta$. Each of these levels is still four-fold degenerate, but this time due to *orbital* and spin degeneracies. Note that we may still use the wave functions quoted earlier even for this case if we adopt the convention that $\phi_{k,n}(y)$ is identically zero if $n < 0$.

Appendix C: Minimization of the ground-state expectation value of the interacting Hamiltonian with an AF order parameter

We now provide details on the calculation and minimization of the ground-state expectation value of the interacting Hamiltonian with an antiferromagnetic order parameter. We start by rewriting the field operators in our Hamiltonian in terms of the eigenstates of the H_0 derived above; the formula for this is given by Equation (134). If we label the positive energy eigenvalues as $E_{k,n,\tau,s} = E_n = \sqrt{n(n-1)\omega_c^2 + \Delta^2}$, then H_0 becomes

$$H_0 = \sum_{k,n,\tau,s} E_{k,n,\tau,s} (a_{k,n,\tau,s}^\dagger a_{k,n,\tau,s} + b_{k,n,\tau,s}^\dagger b_{k,n,\tau,s}) - \sum_{k,n,\tau,s} E_{k,n,\tau,s}. \quad (\text{C1})$$

The expectation value of H_0 with respect to the ground state $|0\rangle$ is then

$$\langle 0 | H_0 | 0 \rangle = - \sum_{k,n,\tau,s} E_{k,n,\tau,s} = -4d \sum_n E_n - 4d|\Delta|, \quad (\text{C2})$$

where d is the degeneracy of each Landau level due to the wave number k .

Now we turn our attention to the interaction, starting with the quadratic term,

$$H_I^{(2)} = \Delta \int d^2\mathbf{r} \psi^\dagger(\mathbf{r})(C_1 \otimes \sigma_z)\psi(\mathbf{r}). \quad (\text{C3})$$

In terms of the eigenstates of H_0 , this becomes

$$H_I^{(2)} = \Delta \int d^2\mathbf{r} \sum_{mn} \psi_m^\dagger(\mathbf{r})(C_1 \otimes \sigma_z)\psi_n(\mathbf{r})a_m^\dagger a_n, \quad (\text{C4})$$

where the Landau level eigenspinors $\psi_n(\mathbf{r})$ in this equation are given by Eq.(B3). Here, we let the indices m and n stand for all of the quantum numbers characterizing a given eigenstate, and we use a_m to stand for either a positive or negative energy state, with the understanding that the negative energy state is given by $a_m = b_m^\dagger$. Upon taking the expectation value of this term with respect to the ground state, we find that only the negative energy states contribute:

$$\langle 0 | H_I^{(2)} | 0 \rangle = \Delta \int d^2\mathbf{r} \sum_{m < 0} \psi_m^\dagger(\mathbf{r})(C_1 \otimes \sigma_z)\psi_m(\mathbf{r}), \quad (\text{C5})$$

where “ $m < 0$ ” means that we only sum over the negative energy states. We may now evaluate all of the sums and integrals using the expressions given above for the wave functions, eventually arriving at

$$\langle 0 | H_I^{(2)} | 0 \rangle = \frac{L_x L_y}{2\pi l_B^2} \Delta^2 \left(\sum_m \frac{1}{E_m} + \sum_{m \geq 2} \frac{1}{E_m} \right), \quad (\text{C6})$$

where $l_B = \sqrt{c/eB}$ is the magnetic length and L_x and L_y are the dimensions of our system. Note that we have two sums, one over all Landau levels, and one only over those with orbital index $m \geq 2$; this is due to the special nature of the $m = 0$ and 1 levels noted earlier.

We now consider the quartic terms. Each of these terms, neglecting the coupling constants and integrals

over position, has the form,

$$[\psi^\dagger(\mathbf{r})S\psi(\mathbf{r})][\psi^\dagger(\mathbf{r})T\psi(\mathbf{r})], \quad (\text{C7})$$

where S and T are matrices. Substituting in Equation (134), and adopting the same conventions as before, this becomes

$$\sum_{mnpq} [\psi_m^\dagger(\mathbf{r})S\psi_n(\mathbf{r})][\psi_p^\dagger(\mathbf{r})T\psi_q(\mathbf{r})]a_m^\dagger a_n a_p^\dagger a_q. \quad (\text{C8})$$

We now take the expectation value of this expression with respect to the ground state. This expectation value will involve the expression, $\langle 0 | a_m^\dagger a_n a_p^\dagger a_q | 0 \rangle$. The only way for this to be non-zero is if m and q are negative-energy states. We must also require that n and p either be both positive-energy states or both negative-energy states. In the former case, we obtain, using the anticommutation relations for fermions,

$$\langle 0 | b_m a_n a_p^\dagger b_q^\dagger | 0 \rangle = \delta_{mq} \delta_{np}.$$

In the latter case, we obtain

$$\langle 0 | b_m b_n^\dagger b_p b_q^\dagger | 0 \rangle = \delta_{mn} \delta_{pq}.$$

Putting these results together, the above quartic form becomes

$$\sum_{m < 0, n > 0} [\psi_m^\dagger(\mathbf{r})S\psi_n(\mathbf{r})][\psi_n^\dagger(\mathbf{r})T\psi_m(\mathbf{r})] + \sum_{m, p < 0} [\psi_m^\dagger(\mathbf{r})S\psi_m(\mathbf{r})][\psi_p^\dagger(\mathbf{r})T\psi_p(\mathbf{r})]. \quad (\text{C9})$$

Evaluation of the above sums and integrals is facilitated by the orthogonality of the Hermite polynomials when the integrals over the momentum quantum number are performed. Finally, using this result, we find that the total energy $E_{\text{var}} = \langle 0 | H | 0 \rangle$ of our system is, noting that $d = L_x L_y / (2\pi l_B^2)$,

$$E_{\text{var}} = -\frac{2L_x L_y}{\pi l_B^2} \sum_n E_n - \frac{2L_x L_y}{\pi l_B^2} |\Delta| + \frac{L_x L_y}{2\pi l_B^2} \Delta^2 \left(\sum_m \frac{1}{E_m} + \sum_{m \geq 2} \frac{1}{E_m} \right) + \frac{L_x L_y}{8\pi^2 l_B^4} V_0 A_{uc} \sum_{mn} \left(1 - \frac{\Delta^2}{E_m E_n} \right) + \frac{L_x L_y}{8\pi^2 l_B^4} V_0 A_{uc} \sum_{m \geq 2, n \geq 2} \left(1 - \frac{\Delta^2}{E_m E_n} \right) + \frac{L_x L_y}{4\pi^2 l_B^4} V_K A_{uc} \sum_{m, n \geq 2} \left(1 - \frac{\Delta^2}{E_m E_n} \right). \quad (\text{C10})$$

We will now minimize this energy with respect to Δ . First, we take the derivative of the above expression, which may be written as

$$\frac{\partial E_{\text{var}}}{\partial \Delta} = \frac{2L_x L_y}{\pi l_B^2} \left[\Delta - \frac{1}{4\pi l_B^2} (V_0 + V_K) A_{uc} \left(\sum_{m \geq 2} \frac{1}{E_m} + \text{sgn} \Delta \right) \right] \sum_{n \geq 2} \frac{1}{E_n} \left(1 - \frac{\Delta^2}{E_n^2} \right). \quad (\text{C11})$$

We now set this derivative to zero. We note that the second factor can never be zero, since $E_n > \Delta$ for all $n \geq 2$, and

therefore it is always positive. We may therefore drop this factor. The remainder, upon simplifying and noting that $l_B = 1/\sqrt{m\omega_c}$, thus yields Equation (135).

-
- ¹ J. Martin, B. E. Feldman, R. T. Weitz, M. T. Allen, and A. Yacoby, *Phys. Rev. Lett.* **105**, 256806 (2010).
 - ² A. S. Mayorov, D. C. Elias, M. Mucha-Kruczyński, R. V. Gorbachev, T. Tudorovskiy, A. Zhukov, S. V. Morozov, M. I. Katsnelson, V. I. Fal'ko, A. K. Geim, and K. S. Novoselov, *Science* **333**, 860 (2011).
 - ³ R. T. Weitz, M. T. Allen, B. E. Feldman, J. Martin, and A. Yacoby, *Science* **330**, 812 (2010).
 - ⁴ J. Velasco Jr., L. Jing, W. Bao, Y. Lee, P. Kratz, V. Aji, M. Bockrath, C. N. Lau, C. Varma, R. Stillwell, D. Smirnov, F. Zhang, J. Jung, and A. H. MacDonald, arXiv:1108.1609 (unpublished).
 - ⁵ O. Vafek and K. Yang, *Phys. Rev. B* **81**, 041401 (2010).
 - ⁶ O. Vafek, *Phys. Rev. B* **82**, 205106 (2010).
 - ⁷ Y. Lemonik, I. L. Aleiner, C. Toke, and V. I. Fal'ko, *Phys. Rev. B* **82**, 201408 (2010).
 - ⁸ A. H. Castro Neto, F. Guinea, N. M. R. Peres, K. S. Novoselov, and A. K. Geim, *Rev. Mod. Phys.* **81**, 109 (2009).
 - ⁹ M. Mucha-Kruczyński, I. L. Aleiner, and V. I. Fal'ko, *Phys. Rev. B* **84**, 041404 (2011).
 - ¹⁰ J. Nilsson, A. H. Castro Neto, N. M. R. Peres, and F. Guinea, *Phys. Rev. B* **73**, 214418 (2006).
 - ¹¹ H. Min, G. Borghi, M. Polini, and A. H. MacDonald, *Phys. Rev. B* **77**, 041407 (2008).
 - ¹² E. V. Castro, N. M. R. Peres, T. Stauber, and N. A. P. Silva, *Phys. Rev. Lett.* **100**, 186803 (2008).
 - ¹³ R. Nandkishore and L. Levitov, *Phys. Rev. Lett.* **104**, 156803 (2010).
 - ¹⁴ R. Nandkishore and L. Levitov, *Phys. Rev. B* **82**, 115124 (2010).
 - ¹⁵ R. Nandkishore and L. Levitov, arXiv:1002.1966 (unpublished).
 - ¹⁶ A. H. MacDonald, J. Jung, and F. Zhang, arXiv:1109.0307 (unpublished).
 - ¹⁷ R. Shankar, *Rev. Mod. Phys.* **66**, 129 (1994).
 - ¹⁸ R. Nandkishore and L. Levitov, *Phys. Rev. B* **81**, 041402 (2010).
 - ¹⁹ C. Hou, C. Chamon, and C. Mudry, *Phys. Rev. Lett.* **98**, 186809 (2007).
 - ²⁰ M. Kharitonov, arXiv:1109.1553 v1 (unpublished).
 - ²¹ J. W. Negele and H. Orland, *Quantum Many-Particle Systems* (Westview Press, 1998), ISBN 0-7382-0052-2.
 - ²² J. Nilsson, A. H. Castro Neto, F. Guinea, and N. M. R. Peres, *Phys. Rev. B* **78**, 045405 (2008).
 - ²³ D. D. L. Chung, *J. Mater. Sci.* **37**, 1 (2002).
 - ²⁴ Wolfram Functions, <http://functions.wolfram.com/09.04.06.0027.01>